NASA Contractor Report 189545

ICASE Report No. 91-69

ICASE

IGNITION AND STRUCTURE OF A LAMINAR DIFFUSION FLAME IN THE FIELD OF A VORTEX

Michéle G. Macaraeg

T. L. Jackson

M. Y. Hussaini

NASA

National Aeronautics and
Space Administration

Langley Research Center
Hampton, Virginia 23665-5225

N92-11162

Unclas

G3/25   0048385

(NASA-CR-189545) IGNITION AND STRUCTURE OF A LAMINAR DIFFUSION FLAME IN THE FIELD OF A VORTEX Final Report (ICASE) 35 p CSCL 21B

ERRATA

NASA Contractor Report 189042

IGNITION AND STRUCTURE OF A LAMINAR
DIFFUSION FLAME IN THE FIELD OF A VORTEX

Michele G. Macaraeg, T. L. Jackson,
and M. Y. Hussaini

September 1991

NASA Contractor Report 189042 has an incorrect report number. The correct report
number is NASA Contractor Report 189545. Please mark your copies on the cover and
Report Documentation Page to reflect this change.

Issued January 1992

IGNITION AND STRUCTURE OF A LAMINAR DIFFUSION FLAME IN THE FIELD OF A VORTEX

Michèle G. Macaraeg

NASA Langley Research Center
Hampton, Virginia 23665

T.L. Jackson

Department of Mathematics and Statistics
Old Dominion University
Norfolk, Virginia 23529

M.Y. Hussaini

Institute for Computer Applications in Science and Engineering
NASA Langley Research Center
Hampton, Virginia 23665

ABSTRACT

The distortion of flames in flows with vortical motion is examined via asymptotic analysis and numerical simulation. The model consists of a constant-density, one-step, irreversible Arrhenius reaction between initially unmixed species occupying adjacent half-planes which are then allowed to mix and react in the presence of a vortex. The evolution in time of the temperature and mass-fraction fields is followed. Emphasis is placed on the ignition time and location as a function of vortex Reynolds number and initial temperature differences of the reacting species. The study brings out the influence of the vortex on the chemical reaction. In all phases, good agreement is observed between asymptotic analysis and the full numerical solution of the model equations.

i

1. INTRODUCTION

In a seminal paper, Marble (1985) developed a simple model problem which describes the distortion of a diffusion flame by the presence of a viscous vortex flow, as might be found in the large scale structures of turbulent diffusion flames. Assuming fast chemical kinetics and the constant density approximation, a flame sheet exists at time zero separating a region of fuel in the upper half plane and a region of oxidizer in the lower half plane. As time increases, the flame sheet is allowed to evolve by diffusion and convection and is wound up by the vortex flow field. The analysis was based on the assumption that the flame elements are locally strained and sheared, but that the shearing motion was unimportant and hence could be neglected. Theoretical analysis shows that (i) the vortex field increases the reactant consumption, (ii) the reaction rate is independent of time, (iii) a similarity rule for the core radius growth exists, and (iv) a similarity rule exists for the reactant consumption rate.

The analytical problem posed by Marble (1985) (henceforth called the Marble problem) has been solved numerically by Laverdant and Candel (1988) and Rehm, Baum, Lozier and Aronson (1989), but without the strain-shear approximation. Thus the complete flow field was considered. Laverdant and Candel (1988) solved the Marble problem by an implicit finite difference scheme. They verified numerically Marble's similarity rule for the core radius growth and the result that the reaction rate is independent of time, and also verified the correctness of the shear approximation. In addition, the effect of varying the stoichiometric (or equivalence) parameter was also studied. They showed that the core is mostly surrounded by the oxidizer when the stoichiometric parameter is less than unity (fuel lean), and is mostly surrounded by the fuel when it is greater than unity (fuel rich). Rehm, et al. (1989) solved the Marble problem by first transforming the system into a Lagrangian coordinate system. Then assuming a similarity solution, the resulting problem was solved analytically using Fourier series. The Fourier amplitudes were determined by either a two-point boundary-value solver, valid for all values of the independent parameters, or in the asymptotic limit of large Schmidt number (as might be more appropriate for liquids than for gases). The results of this study confirmed the behaviour of the numerical solution of Laverdant and Candel (1988), as well as the dependency of the reactant consumption rate found by Marble (1986). Norton (1983) also solved the Marble problem with the strain-shear approximation, but using finite rate chemistry instead of the flame sheet approximation, confirming the results of Marble.

Many extensions of the Marble problem exist, each utilizing the same analytical approach as that of Marble (1985) and assuming the fast chemistry limit, some of which are briefly reviewed here. Karagozian and Marble (1986) considered the time dependent interaction of a diffusion flame with an axially strained vortex in the third dimension. It was shown that the main conclusions for the three dimensional vortex field remains formally identical to the two dimensional vortex field (the Marble problem). In addition, density effects were shown to be small. Karagozian and Manda (1986) considered the distortion of a two dimensional fuel strip in the presence of a pair of counter-rotating vorticies. The fuel strip was assumed either infinite or semi-infinite in extent, separated from the oxidizer by two flame sheets. On each flame sheet resides a vortex, which are allowed to rotate in opposite directions. The semi-infinite fuel strip is particularly relevant to the vortical flame structure formed at a circular orifice or nozzle. Cetegen and Sirignano considered the interaction of a diffusion flame with a single vortex (1987) and the interaction with an infinite row of two dimensional vortices, which is representative of the temporal growth of a mixing layer before pairing has occurred (1988). In both cases, the emphasis was on the construction of the concentration

profiles in the vortical structure, as well as, the construction of the probability density functions (pdfs). A review of these two cases can be found in Sirignano (1989). Peters and Williams (1988) developed an analogous problem for a premixed flame, relevant for describing premixed turbulent combustion in large scale structures. The emphasis of this study was in describing the growth of the reacted core, flame extinction by stretch for Lewis numbers greater than unity, and the effect of heat release.

In another seminal paper, Linan and Crespo (1976) examined the structure of a diffusion flame in the unsteady mixing of two half spaces of fuel and oxidizer. By using a combination of large activation energy asymptotics and numerics, they analyzed the continuous evolution from nearly frozen flow to near equilibrium flow and showed that three laminar regimes exist within the flow; the ignition, deflagration, and diffusion flame regimes. The ignition regime is a region where the combustible gases mix until, at some finite time, a thermal explosion occurs at a well defined location and the gas is ignited. The second regime is the deflagration region. After ignition, a pair of deflagration waves (or "premixed flamelets") emerge according to classical thermal explosion theory. These waves arise because the mixture is not stoichiometric in the premixed region. One of the reactants is consumed locally, leaving behind an excess of the other reactant. Thus, one of the flamelets is fuel-rich and the other is fuel-lean. There is excess fuel behind the fuel-rich flamelet and excess oxidizer behind the fuel-lean flamelet. Concentration gradients behind the flamelets drive the unburnt fuel and oxidizer towards the diffusion flame where they are consumed locally. These premixed flamelets are quite weak in that the temperature rise associated with them is small, and they exist only until all of the deficient reactant is consumed. Just beyond the deflagration waves, a diffusion flame regime exists where the mixing process is governed by diffusion in the direction normal to the flame. As time increases, the diffusion flame approaches a flame sheet. We note that the existence of a well defined ignition point and the premixed flamelets depends critically on the relative magnitudes of the two initial temperatures to that of the adiabatic diffusion flame temperature. That is, if the adiabatic diffusion flame temperature is greater than either initial temperature, a well defined ignition point always occurs, followed by the premixed flamelets. On the other hand, if the adiabatic diffusion flame temperature is between the two initial temperatures, there is no well defined ignition point, and a single premixed flame merges smoothly into the diffusion flame. The analytical results of Linan and Crespo were extended by Jackson and Hussaini (1988) and Grosch and Jackson (1991) in their studies of steady supersonic combustion in compressible laminar mixing layers. In particular, the three flame regimes also exist at high speeds provided the adiabatic diffusion flame temperature is greater than either freestream temperature. Finally, we note that this configuration of two flamelets and a diffusion flame (collectively called a tribrachial flame) has also been observed in the propagation of a premixed flame into a nonuniform mixture (e.g., Buckmaster and Matalon, 1988).

Our goal is to combine the models of Marble (1985) and Linan and Crespo (1976). That is, we propose to investigate the continuous evolution of initially unmixed species occupying adjacent half planes to near equilibrium flow in the presence of a viscous vortex without invoking the fast chemistry limit. Emphasis is placed on the ignition time and location as a function of vortex Reynolds number and initial temperature differences of the reacting species. In the next section we state the problem. Section 3 presents an analysis of the ignition regime using a combination of large activation energy (and hence Zeldovich number) asymptotics and numerics. Section 4 presents a simple model problem for the diffusion flame regime describing the viscous core region about the flame sheet, and identifies certain physical effects by employing asymptotic expansions and numerical solutions. The full equations are then solved numerically

in section 5. Comparisons between asymptotics and numerics are given through out the study. Finally, our conclusions are presented in section 6.

2. EQUATION FORMULATION

In this section the problem for the time evolution of initially unmixed species occupying adjacent half-planes which are then allowed to mix and react in the presence of a vortex is stated. The nondimensional equations, boundary conditions and initial conditions governing this field in cylindrical coordinates are

$$U = 0, \qquad V = \frac{R\,Sc}{r}\,[1 - \exp(-r^2/4\,t\,Sc)], \tag{2.1a}$$

$$T_t + \frac{V}{r}\,T_\theta = \nabla^2 T + \beta\,\Omega, \tag{2.1b}$$

$$F_{j,t} + \frac{V}{r}\,F_{j,\theta} = \nabla^2 F_j - \Omega, \quad j = 1,2, \tag{2.1c}$$

$$\Omega = Da\,F_1 F_2\,e^{-Ze/T}, \tag{2.1d}$$

$$T = F_1 = 1, F_2 = 0 \qquad at \quad t = 0, r > 0, 0 < \theta < \pi, \quad \text{and} \quad t > 0, r \to \infty, 0 < \theta < \pi, \tag{2.2a}$$

$$T = \beta_T, F_1 = 0, F_2 = \frac{F_{2,-\infty}}{F_{1,\infty}} \equiv \phi^{-1} \qquad at \quad t = 0, r > 0, \pi < \theta < 2\pi,$$

$$\text{and} \quad t > 0, r \to \infty, \pi < \theta < 2\pi, \tag{2.2b}$$

where (U,V) are the radial and angular velocity components, respectively; ∇^2 is the two-dimensional Laplacian operator in cylindrical coordinates; T is the temperature; and F_1 and F_2 the mass fractions. The chemical model is a one-step irreversible Arrhenius reaction, and the vortex model is an Oseen vortex with circulation Γ. The nondimensional parameters appearing above are the vortex Reynolds number R, defined as $\Gamma / 2\pi\nu$ where ν is the kinematic viscosity; the Schmidt number $Sc = \nu/D$ assumed equal for both species and D is the species diffusion coefficient; the Zeldovich number $Ze = E / (R^o\,T_\infty)$ with E the dimensional activation energy and R^o the universal gas constant; the Damkohler number Da defined as the ratio of the characteristic diffusion time scale to the characteristic chemical time scale; β the heat release per unit mass of F_1; the equivalence ratio ϕ defined as the ratio of the mass fraction F_1 to the mass fraction F_2 divided by the ratio of their molecular weights times their stoichiometric coefficients; and finally β_T the ratio of the initial temperatures. If $\phi = 1$, the mixture is said to be stoichiometric, if $\phi > 1$ it is F_1 rich, and if $\phi < 1$, it is F_1 lean. Also, if β_T is less than one, F_2 is relatively cold compared to F_1, and if β_T is greater than one it is relatively hot. The temperature and mass fractions were nondimensionalized by the values T_∞ and $F_{1,\infty}$, respectively. The velocities were nondimensionalized by U_o, some characteristic speed. Lengths and times are referred to the relevant diffusion characteristic scales $l_d = \lambda/\rho\,C_p\,U_o$ and l_d / U_o of the flow,

respectively, where ρ is the density assumed constant, λ is the thermal conductivity, and C_p is the specific heat at constant pressure. Finally, the assumption of unit Lewis number is made, so that $Sc = Pr$, where Pr is the Prandtl number.

3. IGNITION REGIME

At time $t = 0$, the reaction rate is exactly zero owing to the product $F_1 F_2 = 0$. For $t > 0$, the fuel and oxidizer begin to mix by diffusion, as well as by convection due to the presence of the vortex, and the reaction rate is no longer zero. For small time, it can reasonably be assumed that the effect of the reaction is small, and in the absence of reaction term the system (2.1) reduces to

$$T_t + \frac{R\,Sc}{r^2}\,[1 - \exp(-r^2/4\,t\,Sc)]\,T_\theta = \nabla^2 T, \tag{3.1a}$$

$$F_{j,t} + \frac{R\,Sc}{r^2}\,[1 - \exp(-r^2/4\,t\,Sc)]\,F_{j,\theta} = \nabla^2 F_j, \quad j = 1,2. \tag{3.1b}$$

The above system must be solved numerically subject to the conditions (2.2), and its solutions are referred to as the inert solutions, denoted by

$$T_I \equiv T_I(r,\theta,t), \qquad F_{j,I} \equiv F_{j,I}(r,\theta,t), \quad j = 1,2. \tag{3.2}$$

As time increases, more of the combustible mixes until, at some finite time, a thermal explosion occurs characterized by significant departure from the inert.

To analyze the ignition process, we determine the effect of the growing reaction rate by expanding about the inert solution as

$$T = T_I + Ze^{-1} T_1, \qquad F_j = F_{j,I} + Ze^{-1} F_{j,1} \quad j = 1,2, \tag{3.3}$$

and take the asymptotic limit $Ze \to \infty$. Substituting into (2.1), we see that the left hand sides are $O(Ze^{-1})$ while the right hand sides are $O(Da\,e^{-Ze/T_*})$, where $T_* = max(T_I)$. In order to balance these terms, Da must therefore have the form

$$Da = \frac{1}{\beta Ze}\,e^{Ze/T_*}. \tag{3.4}$$

Substituting into (2.1b) yields the following equation for T_1

$$T_{1,t} + \frac{R\,Sc}{r^2}\,[1 - \exp(-r^2/4\,t\,Sc)]\,T_{1,\theta} = \nabla^2 T_1$$
$$+ [F_{1,I} + Ze^{-1} F_{1,1}]\,[F_{2,I} + Ze^{-1} F_{2,1}]\,\exp\left[\frac{T_1 + Ze\,(T_I - T_*)}{T_*\,(T_I + Ze^{-1} T_1)}\right], \tag{3.5}$$

which must be solved subject to the initial and boundary conditions

$$T_1 = 0 \quad at \quad t = 0, r > 0, 0 < \theta < 2\pi, \quad \text{and} \quad t > 0, r \to \infty, 0 < \theta < 2\pi. \tag{3.6}$$

Once T_1 is known, the mass fraction perturbations can be found directly from (2.1c). Note that the right hand side of (3.5) is exponentially small except where $|T_I - T_*| \approx O(Ze^{-1})$. There are now two cases to consider, depending upon the magnitude of the parameter $|1 - \beta_T|$. In this section we only consider the case of nearly equal initial temperatures ($\beta_T \approx 1$), and will postpone the analysis for $O(1)$ initial temperature differences as a topic for future research.

As mentioned above, only the important case of ignition for nearly equal initial temperatures of the fuel and oxidizer is considered. To this end, we set

$$\beta_T = 1 + Ze^{-1}\tilde{\beta}_T, \tag{3.7}$$

with $\tilde{\beta}_T$ fixed and $O(1)$. With this choice, the inert temperature T_I is given by

$$T_I = 1 + Ze^{-1} T_{I,1} \tag{3.8}$$

where $T_{I,1}$ satisfies (3.1a) subject to the initial and boundary conditions

$$T_{I,1} = 0 \qquad at \quad t = 0, r > 0, 0 < \theta < \pi, \quad \text{and} \quad t > 0, r \to \infty, 0 < \theta < \pi, \tag{3.9a}$$

$$T_{I,1} = \tilde{\beta}_T \qquad at \quad t = 0, r > 0, \pi < \theta < 2\pi, \quad \text{and} \quad t > 0, r \to \infty, \pi < \theta < 2\pi. \tag{3.9b}$$

Substituting into (3.5), together with the asymptotic choice $T_* = 1$, yields the following equation for the disturbance temperature

$$T_{1,t} + \frac{R\,Sc}{r^2}[1 - \exp(-r^2/4\,t\,Sc)]\,T_{1,\theta} = \nabla^2 T_1 + F_{1,I}\,F_{2,I}\,e^{T_1 + T_{I,1}} \tag{3.10}$$

subject to the conditions (3.6). This equation was solved numerically for a range of R and $\tilde{\beta}_T$ with $Sc = \phi = 1$. Implementation of boundary conditions are facilitated if the system is recast in Cartesian coordinates. The solution technique is a 2nd-order finite difference scheme on a nonuniform mesh. To resolve the structure in the core region of the field, a coordinate stretching of the form

$$y_p = \left[\frac{C_2 - 1}{C_2 - y_c^2}\right]^{C_1} y_{\max} y_c \tag{3.11}$$

is used, where $y_p \in [-y_{max}, y_{max}]$ is the physical coordinate, $y_c \in [-1,1]$ is the computational coordinate, and C_1 and C_2 are adjustable constants. The smaller the quantity $(C_2 - 1)$, the stronger the stretching. In the y direction, C_1 is either 4 or 2, and C_2 is 2. A similar stretching is used in the x direction, with $C_1 = 4$ and $C_2 = 2$. To avoid the singularity at the origin, no mesh points are placed there. The outer boundaries are set at 50 or 200 for x_{max}, and 20 or 50 for y_{max}. Grid resolution studies which at least doubled the computational mesh were carried out to ensure that structures were well resolved. The resolutions required

ranged from a 64^2 mesh to a 256^2 mesh for large vortex Reynolds number (R = 5000). The time-stepping scheme is a four-stage Runge-Kutta which is formally 2nd-order but has an extended stability region making it accurate and robust for moderately stiff problems. All runs were performed interactively on a Cray YMP.

As t increases, the solution for T_1 becomes unbounded at some finite time (t_{ig}) and location (x_{ig}, y_{ig}). This characterizes the ignition regime. The special case $R = 0$, in which two initially unmixed species are allowed to diffuse without the mixing generated by the vortex, corresponds to the results of Linan and Crespo (1976). To verify the solution technique described above, we give a comparison of our results to that of Linan and Crespo in Table I. For this case ignition takes place along a line parallel to the x-axis which is located at $y = 0$ for $\tilde{\beta}_T = 0$ and resides in the hotter region for $\tilde{\beta}_T \neq 0$.

The effects of the vortex can be seen by examining Figures 1 and 2 and Table II. Figure 1 is a plot of the ignition times t_{ig} versus the vortex Reynolds number R for three values of $\tilde{\beta}_T$ with $Sc = \phi = 1$. Table II contains selected ignition times as a function of R for the three values of $\tilde{\beta}_T$ of Figure 1. The effect of increasing $\tilde{\beta}_T$ from zero (i.e., $\beta_T > 1$) is to enhance ignition, while decreasing $\tilde{\beta}_T$ from zero (i.e., $\beta_T < 1$) has the opposite effect. One can see from Figure 1 and Table II that the vortex Reynolds number has little effect on the overall ignition time. However, ignition now occurs at a point rather than along an entire line. This effect is shown in Figure 2 where the ignition locations y_{ig} versus x_{ig} are plotted for various values of R and $\tilde{\beta}_T = -2$. Note that as R increases, the ignition location spirals clockwise towards the viscous core center. Ignition is seen to occur within the core for vortex Reynolds numbers $R > 70$. This is in contrast to the case of equal initial temperatures ($\tilde{\beta}_T = 0$), where ignition always occurs at the origin for any value of R. The analogous plot for $\tilde{\beta}_T = 2$ has essentially the same characteristics as Figure 2. In summary, ignition occurs in the region of the initially hotter reactant for small R, and spirals clockwise towards the viscous core center as R increases.

Figure 2 indicates that the ignition location is at its maximum from the center of the vortex at approximately $R = 28$. Surface plots of T_1 and $F_{1,l}$ shown in Figures 3a,b, respectively, display the skewed structure of the reaction core at these conditions. The development of the hot spot for $\tilde{\beta}_T = -2$ as a function of increasing R is shown in the contour plots of T_1 and $F_{1,l}$ in Figures 4 and 5, respectively. The structure of the reaction core develops from an asymmetrically skewed center (Figures 4a-c) to an axisymmetric center (Figure 4d). However, the local structure of the hot spot within the reaction core is axisymmetric for any value of the vortex Reynolds number greater than zero. This fact is more clearly seen in Figure 6 where we plot T_1 versus y at the ignition location x_{ig} and time t_{ig} corresponding to the same conditions given in Figure 4. From this figure it is clear that once the hot spot develops within the reaction core, it is axisymmetric.

For completeness, a contrast of the effects of a potential vortex distribution ($V = R\,Sc\,/\,r$) versus the Oseen vortex, given in (2.1a), on the ignition locations are made. Figure 7 is a plot of y_{ig} versus x_{ig} for the potential vortex for the same conditions as in Figure 2. Note that the collapse of the spiral into the center occurs for $R > 7$, as opposed to the value $R > 70$ for the Oseen vortex.

The numerical solutions presented above suggests that near thermal runaway, a hot spot develops at (r_{ig}, θ_{ig}) within the reaction core and that the structure of this hot spot is axisymmetric (see Figure 6). Thus, convection is not important and the local structure of the hot spot is diffusion controlled. In this case, Dold (1985, 1989) has shown that the proper scalings characterizing the local structure of the hot spot are given by

$$x = r_{ig} \cos\theta_{ig} + \mu(\tau)s \cos\bar{\theta}, \quad y = r_{ig} \sin\theta_{ig} + \mu(\tau)s \sin\bar{\theta}, \quad \tau = t_{ig} - t, \tag{3.12}$$

where

$$\mu^2(\tau) = \tau[\alpha - \ln(\Omega_{ig}\tau)] \equiv \tau\xi, \tag{3.13}$$

as $\tau \to 0$, with $\Omega_{ig} = F_{1,I}F_{2,I}e^{T_{I,1}}$ evaluated at $(r,\theta,t) = (r_{ig},\theta_{ig},t_{ig})$, and α is a constant determined by matching with the initial conditions and is a function of the parameters (R,Sc,ϕ). With these scalings, and ignoring all dependence on $\bar{\theta}$, the asymptotic form of T_1 in the hot spot is given by

$$T_1 = -\ln(\Omega_{ig}\tau) - \ln(1 + s^2/4) - \frac{\ln\xi}{\xi}\frac{5 + \hat{n}}{2}\frac{s^2/4}{1 + s^2/4}$$

$$+ \frac{1}{\xi}\left[\frac{1 + \hat{n}}{2} - \frac{s^2/4}{1 + s^2/4}\ln(1 + s^2/4)\right] + O(\frac{\ln^2\xi}{\xi^2}), \tag{3.14}$$

with $\hat{n} = 0$ if $r_{ig} \neq 0$ or $\hat{n} = 1$ if $r_{ig} = 0$. Again note that the local structure of the hot spot, once it develops, is independent of the influence of the vortex and so is diffusion controlled. We are currently investigating the future time development of the hot spot, and the subsequent flame development.

4. DIFFUSION FLAME REGIME

Typically, a diffusion flame is characterized by a chemical reaction time that is much smaller than a characteristic diffusion time. Chemical reactions then occur in a narrow zone between the fuel and the oxidizer, where the concentrations of both reactants are very small. Mathematically, the assumption of very fast chemical reaction rates leads to the limit of infinite Damkohler number which reduces the diffusion flame to a flame sheet (i.e., local chemical equilibrium). This assumption significantly reduces the complexity of the problem since it eliminates the analysis associated with the chemical kinetics. For many flows, the assumption of local chemical equilibrium adequately predicts the location and the shape of the diffusion flame (Buckmaster and Ludford, 1982; Williams, 1985). Since the flame sheet model is amenable to analysis, we give its structure below. For finite values of the Damkohler number, equations (2.1) must be solved numerically and this is done in the next section.

We begin the analysis of the diffusion flame regime by defining the following conserved variables (see, e.g.; Williams, 1985):

$$T + \beta F_1 = \beta_T + (1 - \beta_T + \beta)Z, \tag{4.1}$$

$$T + \beta F_2 = \beta_T + \beta\phi^{-1} + (1 - \beta_T - \beta\phi^{-1})Z, \tag{4.2}$$

$$Z = \frac{F_1 - F_2 + \phi^{-1}}{1 + \phi^{-1}}, \tag{4.3}$$

where Z is the mixture mass fraction and satisfies the convection-diffusion equation

$$Z_t + \frac{R\,Sc}{r^2}\,[1 - \exp(-r^2/4\,t\,Sc)]Z_\theta = \nabla^2 Z, \tag{4.4}$$

subject to the initial and boundary conditions

$$Z = 1 \qquad at \quad t = 0, r > 0, 0 < \theta < \pi, \quad \text{and} \quad t > 0, r \to \infty, 0 < \theta < \pi, \tag{4.5a}$$

$$Z = 0 \qquad at \quad t = 0, r > 0, \pi < \theta < 2\pi, \quad \text{and} \quad t > 0, r \to \infty, \pi < \theta < 2\pi. \tag{4.5b}$$

In the limit of infinite Damkohler number the flame sheet solution is given by

$$F_1 = 1 - (1 + \phi^{-1})(1 - Z), \qquad F_2 = 0, \tag{4.6a}$$

$$T = \beta_T + \beta\phi^{-1} + (1 - \beta_T - \beta\phi^{-1})Z, \tag{4.6b}$$

valid for $Z > Z_f$, and

$$F_1 = 0, \qquad F_2 = \phi^{-1} - (1 + \phi^{-1})Z, \tag{4.7a}$$

$$T = \beta_T + (1 - \beta_T + \beta)Z, \tag{4.7b}$$

valid for $Z < Z_f$. Here, Z_f defines the location of the flame sheet where both the reactants vanish, given by the implicit relation

$$Z_f = \frac{1}{1 + \phi}, \tag{4.8a}$$

and T takes the adiabatic flame value

$$T_f = \frac{1 + \beta_T\,\phi + \beta}{1 + \phi}. \tag{4.8b}$$

Note that the flame location is independent of β_T and β. Once $Z = Z(r,\theta,t)$ is known, then the other variables (T, F_1, F_2) can be found from (4.6)-(4.7).

As discussed in the Introduction, equation (4.4) for Z has been solved numerically by Laverdant and Candel (1988) and Rehm, Baum, Lozier and Aronson (1989). Our goal is not the numerical solution of (4.4). Rather, we propose in the following subsections a simple model problem describing the viscous core center in a region about the flame sheet, with the goal of identifying certain physical effects by employing asymptotic expansions.

4.1. LOCAL ANALYSIS ABOUT FLAME SHEET

In this section we formulate a model problem describing the effect of the vortex in a neighborhood about the flame sheet. Assume at time $t = 0$ a flame sheet exists at y_f. In the absence of a vortex, the mixture mass fraction evolves according to (4.4) with $R = 0$, and the analytical solution can be written in terms of an error function. At any instantaneous time t_o, the solution across the flame sheet is easily seen to be a linear shear profile (Figure 8), given by

$$Z(r,\theta,t_o) = \frac{1}{1+\phi} + Z_f'(t_o)(y - y_f(t_o)), \tag{4.9}$$

which is only the first-order Taylor series expansion of the mixture mass fraction profile Z about the flame sheet location y_f, found implicitly by (4.8a). Here, the prime denotes differentiation with respect to y. The model problem assumes that the time scale associated with the vortex is faster than that of diffusion, so that on this time scale the linear profile (4.9) can be considered steady. In addition, we assume that the flame sheet resides close to the origin. Thus the following scales can be introduced

$$t = t_o + \varepsilon \hat{t}, \quad y = \sqrt{\varepsilon}\,\hat{y}, \quad r = \sqrt{\varepsilon}\,\hat{r}, \quad \phi = 1 + \sqrt{\varepsilon}\,\hat{\phi}, \quad Z = \frac{1}{2} + \sqrt{\varepsilon}\,\bar{Z}, \tag{4.10}$$

with $\varepsilon \ll 1$, and the vortex is turned on at time $\hat{t} = 0$. With these scalings the linear shear profile, in terms of $\bar{Z}$, becomes

$$\bar{Z}(\hat{r},\theta,0) = -\frac{\hat{\phi}}{4} + Z_f'(t_o)[\hat{y} - \hat{y}_f(t_o)] \equiv k_1 + k_2\hat{y}. \tag{4.11}$$

Note that $k_1 = -\hat{\phi}/4 - Z_f'(t_o)\hat{y}_f(t_o)$ measures the instantaneous deviation of Z from its stoichiometric value $Z_f = 1/2$ at $\hat{t} = 0$, and $k_2 = Z_f'(t_o)$ measures the instantaneous gradient of the mixture mass fraction across the flame sheet. The convection-diffusion equation (4.4) in terms of the perturbation mixture mass fraction $\bar{Z}$ becomes

$$\bar{Z}_{\hat{t}} + \frac{R\,Sc}{\hat{r}^2}[1 - \exp(-\hat{r}^2/4\hat{t}\,Sc)]\bar{Z}_\theta = \hat{\nabla}^2\bar{Z}, \tag{4.12}$$

where $\hat{\nabla}^2$ is the Laplacian operator in the transformed plane. The perturbation equation (4.12) is to be solved subject to the initial and boundary condition given by the linear shear profile (4.11).

To examine the time evolution of the flame sheet about the origin when the vortex is present, we define

$$\bar{Z}(\hat{r},\theta,\hat{t}) = k_1 + k_2[\hat{r}\sin\theta + \hat{Z}(\hat{r},\theta,\hat{t})], \tag{4.13}$$

where $\hat{Z}$ is the disturbed mass fraction due to the presence of the vortex. Upon substituting (4.13) into (4.12), we find that $\hat{Z}$ satisfies the convection-diffusion equation

$$\hat{Z}_{\hat{t}} + \frac{R\,Sc}{\hat{r}^2}\,[1 - \exp(-\hat{r}^2/4\,\hat{t}\,Sc)]\,(\hat{r}\cos\theta + \hat{Z}_\theta) = \hat{\nabla}^2\hat{Z}, \tag{4.14}$$

subject to homogeneous initial and boundary conditions. Note that (4.14) is non-homogeneous, and hence does not have a similarity solution. Here, we introduce the variable

$$s = \frac{\hat{r}}{\sqrt{\hat{t}}}, \tag{4.15}$$

which is the similarity variable in the absence of the vortex, so that $\hat{Z} \equiv \hat{Z}(s,\theta,\hat{t})$. In the transformed plane $\hat{Z}$ satisfies

$$\hat{t}\,\hat{Z}_{\hat{t}} - \frac{s}{2}\hat{Z}_s + \frac{R\,Sc}{s^2}\,[1 - \exp(-s^2/4\,Sc)]\,(s\,\sqrt{\hat{t}}\cos\theta + \hat{Z}_\theta) = \hat{\nabla}^2\hat{Z}. \tag{4.16}$$

This equation is separable in space and time and hence has the simple analytical solution

$$\hat{Z} = \sqrt{\hat{t}}\,[\hat{Z}_e(s)\cos\theta + \hat{Z}_o(s)\sin\theta], \tag{4.17}$$

where

$$\frac{1}{2}(\hat{Z}_e - s\,\hat{Z}'_e) + \frac{R\,Sc}{s^2}\,[1 - \exp(-s^2/4\,Sc)]\,(\hat{Z}_o + s) = \hat{Z}''_e + \frac{1}{s}\hat{Z}'_e - \frac{1}{s^2}\hat{Z}_e, \tag{4.18}$$

$$\frac{1}{2}(\hat{Z}_o - s\,\hat{Z}'_o) - \frac{R\,Sc}{s^2}\,[1 - \exp(-s^2/4\,Sc)]\hat{Z}_e = \hat{Z}''_o + \frac{1}{s}\hat{Z}'_o - \frac{1}{s^2}\hat{Z}_o, \tag{4.19}$$

subject to the boundary conditions

$$\hat{Z}_e(0) = \hat{Z}_o(0) = \hat{Z}_e(\infty) = \hat{Z}_o(\infty) = 0. \tag{4.20}$$

Here, primes denote ordinary differentiation with respect to the similarity variable s, $\hat{Z}_e$ is the amplitude of the even mode, and $\hat{Z}_o$ is the amplitude of the odd mode. Note that the above solution is valid for all times and vortex Reynolds numbers.

The system (4.18-4.19) subject to (4.20) was solved numerically using a 2nd-order finite difference scheme with an appropriate stretching in s. The solution to this system for a range of vortex Reynolds numbers is given in Figure 9. As the vortex Reynolds number increases, the number of oscillations in each of the components $\hat{Z}_e$ and $\hat{Z}_o$ also increases while moving away from the origin, thus establishing a core region. The composite solution (4.13) is plotted in Figure 10 for $\hat{t} = 1$, $\theta = \pm\pi/2$, $k_2 = 1$, $k_1 = 0$, and $Sc = 1$. From this figure the extent of the core region is seen to grow as R increases, and this core, once established, grows like $\sqrt{\hat{t}}$ (see (4.17)) as noted previously by Marble (1985).

4.2. LARGE TIME BEHAVIOUR

To investigate the local structure of the model problem described in the previous section for large times, let $\hat{t} \to \infty$, so that $s \to 0$ for fixed $\hat{r}$. Hence from (4.17) we have

$$\hat{Z} = \lim_{\hat{t} \to \infty} \sqrt{\hat{t}} \, [\hat{Z}_e(s) \cos\theta + \hat{Z}_o(s) \sin\theta]$$

$$= \lim_{s \to 0} \frac{\hat{r}}{s} [\hat{Z}_e(s) \cos\theta + \hat{Z}_o(s) \sin\theta]$$

$$= \lim_{s \to 0} \frac{1}{s} [\hat{Z}_e(s)\hat{x} + \hat{Z}_o(s)\hat{y}]$$

$$= a_1 \hat{x} + b_1 \hat{y}, \tag{4.21}$$

where from (4.18) and (4.19) it is easy to show that the asymptotic behaviour as $s \to 0$ is

$$\hat{Z}_e = a_1 s + O(s^3), \qquad \hat{Z}_o = b_1 s + O(s^3). \tag{4.22}$$

Here, a_1 and b_1 are to be found numerically. Substituting (4.22) into (4.13) yields

$$\bar{Z} = k_1 + k_2 [a_1 \hat{x} + (1 + b_1)\hat{y}]. \tag{4.23}$$

Comparing (4.23) to (4.11), the effect of the vortex is seen to establish a new equilibrium mixture mass fraction profile within the core region.

Another quantity of interest is the magnitude of the gradient of the mixture mass fraction, defined as

$$G = \left[\left[\frac{\partial Z}{\partial x} \right]^2 + \left[\frac{\partial Z}{\partial y} \right]^2 \right]^{1/2}. \tag{4.24}$$

Note that G is a function of R, ϕ and Sc. Substituting (4.23) into (4.24), we see that the magnitude of the gradient in the center of the core is given by

$$G = |k_2| \left[a_1^2 + (1 + b_1)^2 \right]^{1/2}. \tag{4.25}$$

Figure 11 is a plot of G versus R for $Sc = \phi = k_2 = 1$. Note that as $R \to \infty$, $G \to 0$ which implies that there are no gradients within the center of the core, and hence no diffusion across it. Thus, the core is completely established. From this figure it is clear that the core is 95% established at $R \approx 50$. This is in agreement with Figure 10 where a well defined core is clearly visible at $R = 100$.

4.3. LARGE VORTEX REYNOLDS NUMBER ASYMPTOTICS

To investigate the local structure of the model problem described in Section 4.1 at large vortex Reynolds numbers with $R \gg 1$, we begin with the equation

$$\bar{Z}_{\hat{t}} + \frac{1}{\bar{r}^2} [1 - \exp(-R\,\bar{r}^2/4\,\hat{t})]\bar{Z}_\theta = \frac{1}{Sc\,R}\,\hat{\nabla}^2\bar{Z}, \tag{4.26}$$

which is (4.12) with $\hat{r}$ scaled as $\hat{r} = \bar{r}\sqrt{Sc\,R}$. The above equation is solved subject to the initial and boundary conditions

$$\bar{Z} = k_1 + k_2\hat{y} \qquad at \;\; \hat{t} > 0, \bar{r} \to \infty, 0 < \theta < 2\pi, \;\; and \;\; \hat{t} = 0, \bar{r} > 0, 0 < \theta < 2\pi. \tag{4.27}$$

OUTER INVISCID SOLUTION -- $\bar{Z}^O$

In the limit $R \to \infty$, an outer inviscid region exists and is governed by the following inviscid version of (4.26),

$$\bar{Z}^0_{\hat{t}} + \frac{1}{\bar{r}^2}\bar{Z}^0_\theta = 0, \tag{4.28}$$

where $\bar{Z}^O$ denotes the mixture mass fraction in the outer inviscid region. This equation is valid for $\bar{r} = O(1)$ and $\hat{t} \ll O(R)$, so that the effect of a potential line vortex or an Oseen vortex is the same. The solution is easily found by the method of characteristics and is given by

$$\bar{Z}^0 = k_1 + k_2\,\bar{r}\sin\theta_0, \tag{4.29}$$

where θ_0 is the characteristic

$$\theta_0 = \theta - \frac{\hat{t}}{\bar{r}^2}. \tag{4.30}$$

INNER SOLUTION -- $\bar{Z}^I$

As $\bar{r} \to 0$, the solution (4.29) becomes singular so the viscous terms in (4.26) must be retained. We introduce the similarity type variable

$$s = \frac{\bar{r}}{\sqrt{\delta t}}, \tag{4.31}$$

where $\delta \ll 1$ and will be chosen in the course of the analysis. Defining $\bar{Z}^I$ to be the inner variable, and expanding

$$\bar{Z}^I = k_1 + k_2 \sqrt{\delta t} \; \bar{Z}(s, \theta), \tag{4.32}$$

we see that $\bar{Z}$ satisfies the convection-diffusion equation

$$\tfrac{1}{2}(\bar{Z} - s \bar{Z}_s) + \frac{1}{\delta s^2} [1 - \exp(-R \, \delta s^2/4)] \bar{Z}_\theta = \frac{1}{\delta Sc \, R} \nabla^2 \bar{Z}. \tag{4.33}$$

To facilitate matching with the outer inviscid solution (4.29), we change to a new (non-orthogonal) coordinate system in which the characteristic θ_0 is one of the coordinates. Thus, the above equation in terms of s and θ_0 becomes

$$\tfrac{1}{2}(\bar{Z} - s \bar{Z}_s) - \frac{1}{\delta s^2} \exp(-R \, \delta s^2/4) \bar{Z}_{\theta_0}$$

$$= \frac{1}{\delta Sc \, R} \left\{ \left[\frac{\partial}{\partial s} + \frac{2}{\delta s^3} \frac{\partial}{\partial \theta_0} \right]^2 + \frac{1}{s} \left[\frac{\partial}{\partial s} + \frac{2}{\delta s^3} \frac{\partial}{\partial \theta_0} \right] + \frac{1}{s^2} \frac{\partial^2}{\partial \theta_0^2} \right\} (\bar{Z}). \tag{4.34}$$

To balance both sides we must choose

$$1 = \frac{1}{\delta R \, Sc} \frac{1}{\delta^2}, \tag{4.35}$$

or, in terms of δ,

$$\delta = (R \, Sc)^{-1/3}. \tag{4.36}$$

For this scaling, $\exp(-R \, \delta s^2/4)$ is exponentially small in the limit $R \to \infty$, and so again the effect of a potential line vortex or an Oseen vortex is the same. The leading order equation in a δ-expansion is given by

$$\tfrac{1}{2}(\bar{Z} - s \bar{Z}_s) = \frac{4}{s^6} \bar{Z}_{\theta_0 \theta_0}. \tag{4.37}$$

This equation can be solved by separation of variables and, after matching with the outer solution (4.29), the solution is found to be

$$\bar{Z} = s \exp\left[\frac{-4}{3 s^6} \right] \sin \theta_0. \tag{4.38}$$

The inner viscous solution is now given by

$$\bar{Z}^I = k_1 + k_2 \, s \, \sqrt{\delta \hat{t}} \, \exp\left[\frac{-4}{3 s^6} \right] \sin \theta_0. \tag{4.39}$$

COMPOSITE SOLUTION

The composite solution

$$\bar{Z} = k_1 + k_2 \, \bar{r} \exp\left[\frac{-4 (\delta \hat{t})^3}{3 \bar{r}^6} \right] \sin\left[\theta - \frac{\hat{t}}{\bar{r}^2} \right], \tag{4.40}$$

is valid for times $\hat{t} \ll \delta^{-1}$. Figure 12 displays the composite solution $\bar{Z}$ versus s for $\theta = \pm \pi/2$, with $k_1 = 0.5$, $k_2 = 1$, $\delta = 0.05$, and $\hat{t} = 1$. Note the agreement with the numerical solution given in Figure 10.

The magnitude of the gradient of the mixture mass fraction can be obtained by substituting (4.40) into (4.24). Then as $\delta \to 0$, the leading order result yields

$$G = \frac{2 |k_2|}{\delta s^2} \exp\left[\frac{-4}{3 s^6} \right] \left| \cos\left(\theta - \frac{1}{\delta s^2} \right) \right|. \tag{4.41}$$

Figure 13 is a plot of G versus s for $\theta = \pi/2$, $k_2 = 1$, and $\delta = 1/10$. Note that the maximum amplification is about δ^{-1}. The limit $R \to 0$ corresponds to $G \to 0$, and so the large spikes have been created by the vortex.

The core radius growth can be determined from (4.31) and (4.36), and is found to be

$$\frac{\bar{r}}{\sqrt{(Re \; Sc)^{-1/3} \hat{t}}} = constant, \tag{4.42}$$

or, in terms of dimensional quantities (denoted by stars),

$$\frac{r^*}{\sqrt{\Gamma^{*2/3} D^{*1/3} t^*}} = constant. \tag{4.43}$$

This is the main result of Marble (1985), who showed $constant = 0.5092 + O(\sqrt{D^*/\Gamma^*})$. Finally, we note from (4.43) that the spreading of the viscous core due to the vortex field is $(\Gamma^*/D^*)^{2/3}$ times as large as that obtained from diffusion alone in the absence of the vortex, as previously pointed out by Marble (1985) and Karagozian and Marble (1986).

5. NUMERICAL SOLUTION

In this section we present selected numerical results to the full system (2.1) subject to (2.2). This system was solved by a standard finite difference scheme, as previously described in Section 3. To illustrate the numerical solution of (2.1-2.2) of the continuous evolution from nearly frozen flow to near equilibrium flow, we produce here one result corresponding to the case $Sc = \phi = 1$, $R = 28$, $Ze = 30$, $Da = e^{30}/30$, $\beta = 1$, and $\beta_T = 1 - 2/30$. This case corresponds to the asymptotic results of Section 3 as displayed in Figures 3-6. Figure 14a is a plot of the time slices of the temperature profile T, while Figure 14b is a plot of the time slices of the reaction rate term Ω. Time increases from the bottom left corner to the top right corner. In Figure 14a, a hot spot develops initially within the viscous core (frame 1) and rapidly develops into an isolated, almost circular flame which grows as time increases (frames 2-8). At a later time (frame 7) two diffusion flames are clearly visible at the edges of the plot, and as time increases further (frame 8) they move towards the viscous core. Eventually the two diffusion flames will merge with the expanding, almost circular flame located in the viscous core region. Figure 14b shows corresponding results for the reaction rate term. Initially (frame 1) a single isolated point in the rate term is visible. As time increases (frames 2-8) this single point develops into an almost circular ring and spreads in time, leaving within it the burnt core. The reaction rates of the two diffusion flames are given in frames (7-8).

6. CONCLUSIONS

The distortion of flames in flows with vortical motion has been examined by means of asymptotic analysis and numerical simulation. The model consisted of a constant-density, one-step, irreversible Arrhenius reaction between initially unmixed species occupying adjacent half-planes which were then allowed to mix and react in the presence of a vortex. The continuous evolution of the temperature and mass fraction fields from initially unmixed to near equilibrium flow was followed. Emphasis was placed on the ignition time and location as a function of vortex Reynolds number and initial temperature differences of the reacting species. In the ignition regime, the case of near equal initial temperatures was considered. The effect of increasing the initial temperature ratio β_T slightly from unity was to enhance ignition for any fixed vortex Reynolds number R, while decreasing β_T slightly from unity had the opposite effect. However, for fixed β_T, increasing the vortex Reynolds number from zero had little effect on the overall ignition time. The ignition location occurred in the region of the initially hotter reactant for small R, and was seen to spiral clockwise towards the viscous core center as R increases. Finally, numerical solutions of the ignition equations indicated that the hot spot was both axisymmetric and diffusion controlled for any non-zero vortex Reynolds number. Thus, the asymptotic analysis of Dold (1985, 1989) could be used in describing this local structure. The case of different initial temperatures, and the future time development of the hot spot, will be considered in a future manuscript.

In the diffusion flame regime, a simple model problem was proposed to investigate the effect of the vortex on the flame sheet. The model consisted of assuming that the time scale of the vortex was faster than that of diffusion alone, so that on this time scale appropriate asymptotic expansions were used in describing the interaction about the flame sheet. This model problem allowed for the full vortex flow field without making the strain-shear approximation of Marble (1985). Many of the conclusions of Marble (1985) were

verified, including the similarity rule for the core radius growth in the limit of large vortex Reynolds number.

REFERENCES

Buckmaster, J.D. & Ludford, G.S.S. (1982) *Theory of Laminar Flames*. Cambridge University Press, Cambridge.

Buckmaster, J.D. & Matalon, M. (1988) Anomalous Lewis Number Effects in Tribrachial Flames. Twenty-Second Symposium (International) on Combustion, The Combustion Institute, pp. 1527-1535.

Cetegen, B.M. and Sirignano, W.A. (1987) Study of Mixing and Reaction in the Field of a Vortex. Joint Meeting of the Combustion Institute Western States and Japanese Sections, Paper 3B-44, Honolulu, Hawaii.

Cetegen, B.M. and Sirignano, W.A. (1988) Study of Molecular Mixing and a Finite Rate Chemical Reaction in a Mixing Layer. Twenty-Second Symposium (International) on Combustion, The Combustion Institute, pp. 489-494.

Dold, J.W. (1985) Analysis of the Early Stage of Thermal Runaway. Quart. J. Mech. Appl. Math., 38, pp. 361-387.

Dold, J.W. (1989) Analysis of Thermal Runaway in the Ignition Process. SIAM J. Appl. Math., 49, pp. 459-480.

Grosch, C.E. and Jackson, T.L. (1991) Ignition and Structure of a Laminar Diffusion Flame in a Compressible Mixing Layer with Finite Rate Chemistry. Phys. Fluids A, (in press).

Jackson, T.L. & Hussaini, M.Y. (1988) An Asymptotic Analysis of Supersonic Reacting Mixing Layers. Comb. Sci. and Tech., 57, pp. 129-140.

Karagozian, A.R. & Manda, B.V.S. (1986) Flame Structure and Fuel Consumption in the Field of a Vortex Pair. Comb. Sci. and Tech., 49, PP. 185-200.

Karagozian, A.R. & Marble, F.E. (1986) Study of a Diffusion Flame in a Stretched Vortex. Comb. Sci. and Tech., 45, PP. 65-84.

Laverdant, A.M. & Candel, S.M. (1988) A Numerical Analysis of a Diffusion Flame-Vortex Interaction. Comb. Sci. and Tech., 60, pp. 79-96.

Linan, A. & Crespo, A. (1976) An Asymptotic Analysis of Unsteady Diffusion Flames for Large Activation Energies. Comb. Sci. and Tech., 14, pp. 95-117.

Marble, F.E. (1985) Growth of a Diffusion Flame in the Field of a Vortex. in *Recent Advances in Aerospace Sciences*, ed. by C. Cassci, pp. 395-413.

Norton, O.P. (1983) The Effects of a Vortex Field on Flame with Finite Reaction Rates. Ph.D. Thesis, California Institute of Technology, Pasadena, CA.

Peters, N. and Williams, F.A. (1988) Premixed Combustion in a Vortex. Twenty-Second Symposium (International) on Combustion, The Combustion Institute, pp. 495-503.

Rehm, R.G., Baum, H.R., Lozier, D.W., & Aronson, J. (1989) Diffusion-Controlled Reaction in a Vortex Field. Comb. Sci. and Tech., 66, pp. 293-317.

Sirignano, W.A. (1989) Review of Theory of Mixing and Reaction within a Vortical Structure. in *Numerical Combustion*, Lecture Notes in Physics, 351, A. Dervieux and B. Larrouturou (eds.), Springer-Verlag, pp. 440-449.

Williams, F. A. (1985) *Combustion Theory*, 2nd Ed., The Benjamin/Cummings Pub. Co., Menlo Park, Ca.

Table I. IGNITION TIMES for R = 0			
	$\tilde{B}_T = -10$	$\tilde{B}_T = -2$	$\tilde{B}_T = 0$
present study	54.912	13.146	5.813
Linan & Crespo	55.23	13.14	5.81

Table II. IGNITION TIMES vs VORTEX REYNOLDS NUMBER (R)			
R	$\tilde{B}_T = -2$	$\tilde{B}_T = 0$	$\tilde{B}_T = 2$
0	13.148	5.816	1.779
5	12.659	5.632	1.714
10	11.881	5.278	1.6094
20	11.378	4.793	1.541
30	11.559	4.586	1.566
40	11.680	4.443	1.582
50	11.659	4.362	1.580
60	11.598	4.314	1.572
70	11.535	4.313	1.570
80	11.480	4.286	1.582
90	11.436	4.265	1.577
100	11.398	4.231	1.545
200	11.203	4.162	1.544
300	11.122	4.128	1.533
400	11.075	4.108	1.526
500	11.044	4.095	1.506
1000	10.960	4.067	1.506
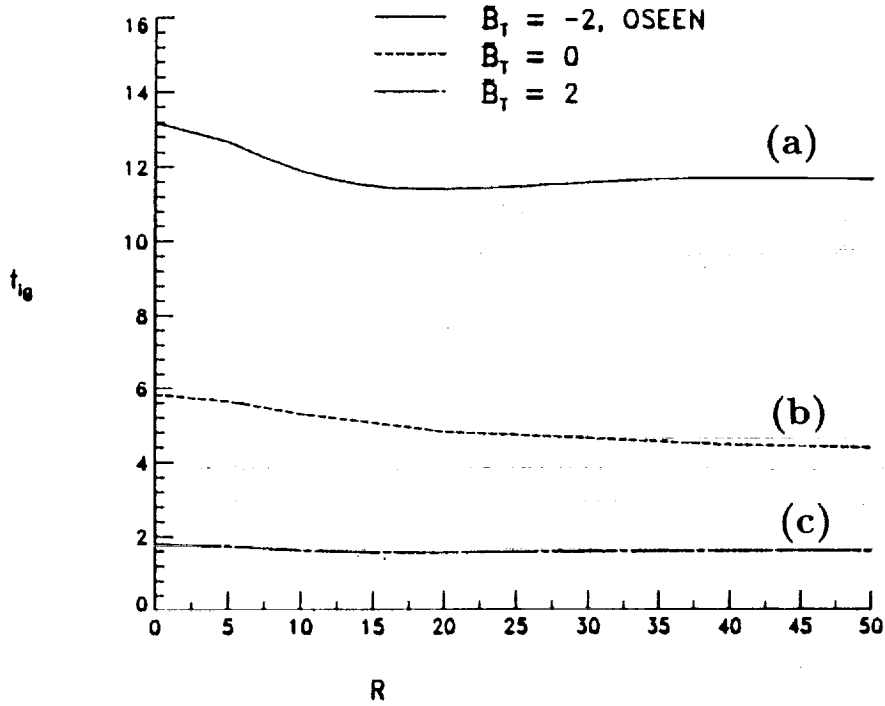
Figure 1. Plot of the ignition time t_{ig} versus vortex Reynolds number R for $Sc = \phi = 1$ and (a) $\tilde{\beta}_T = -2$, (b) $\tilde{\beta}_T = 0$, and (c) $\tilde{\beta}_T = 2$.
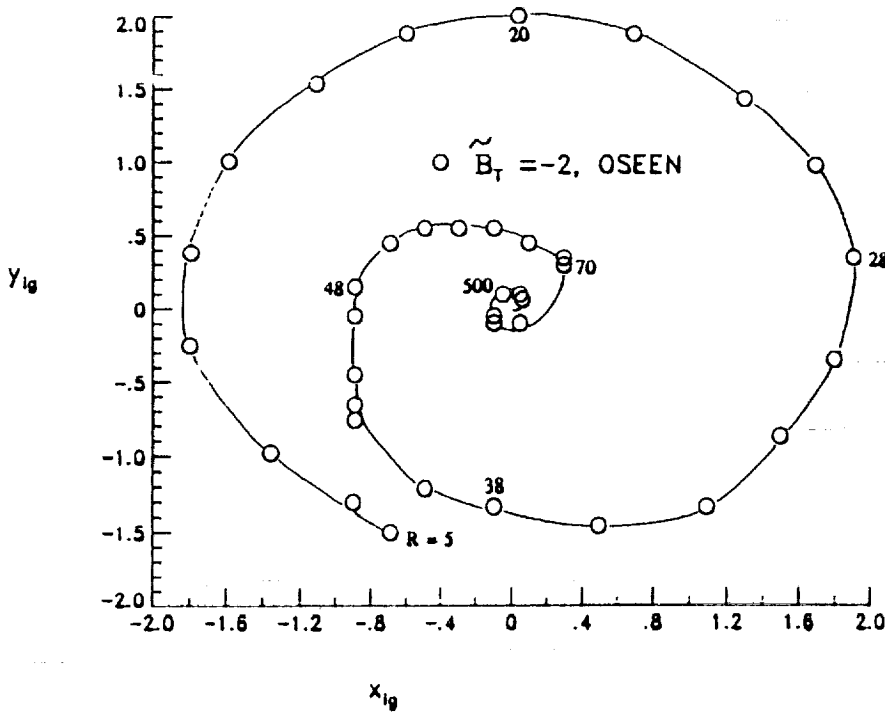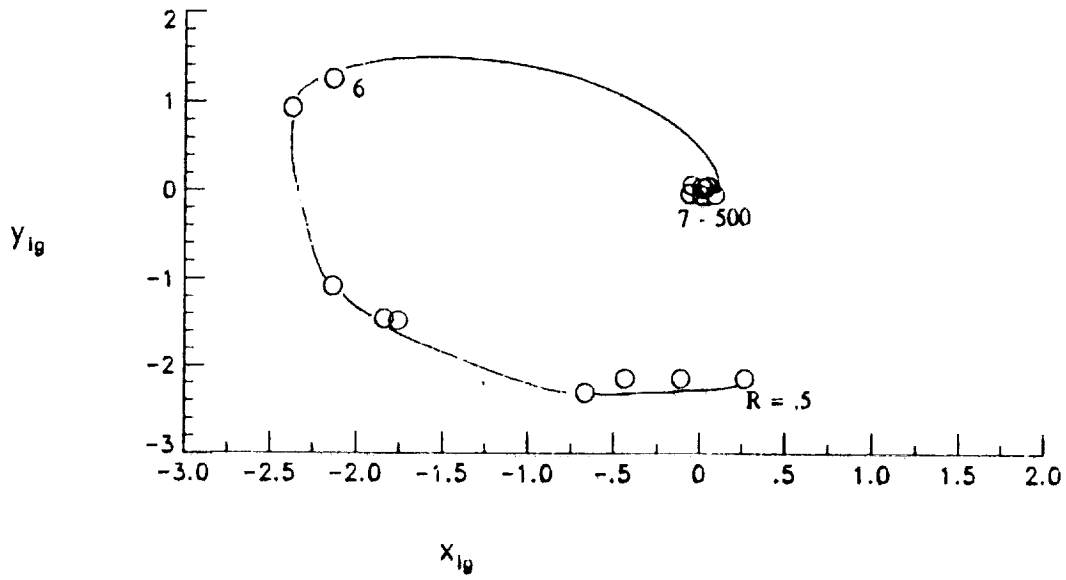

Figure 2. Plot of the ignition locations y_{ig} versus x_{ig} for various values of the vortex Reynolds number with $Sc = \phi = 1$ and $\tilde{\beta}_T = -2$.
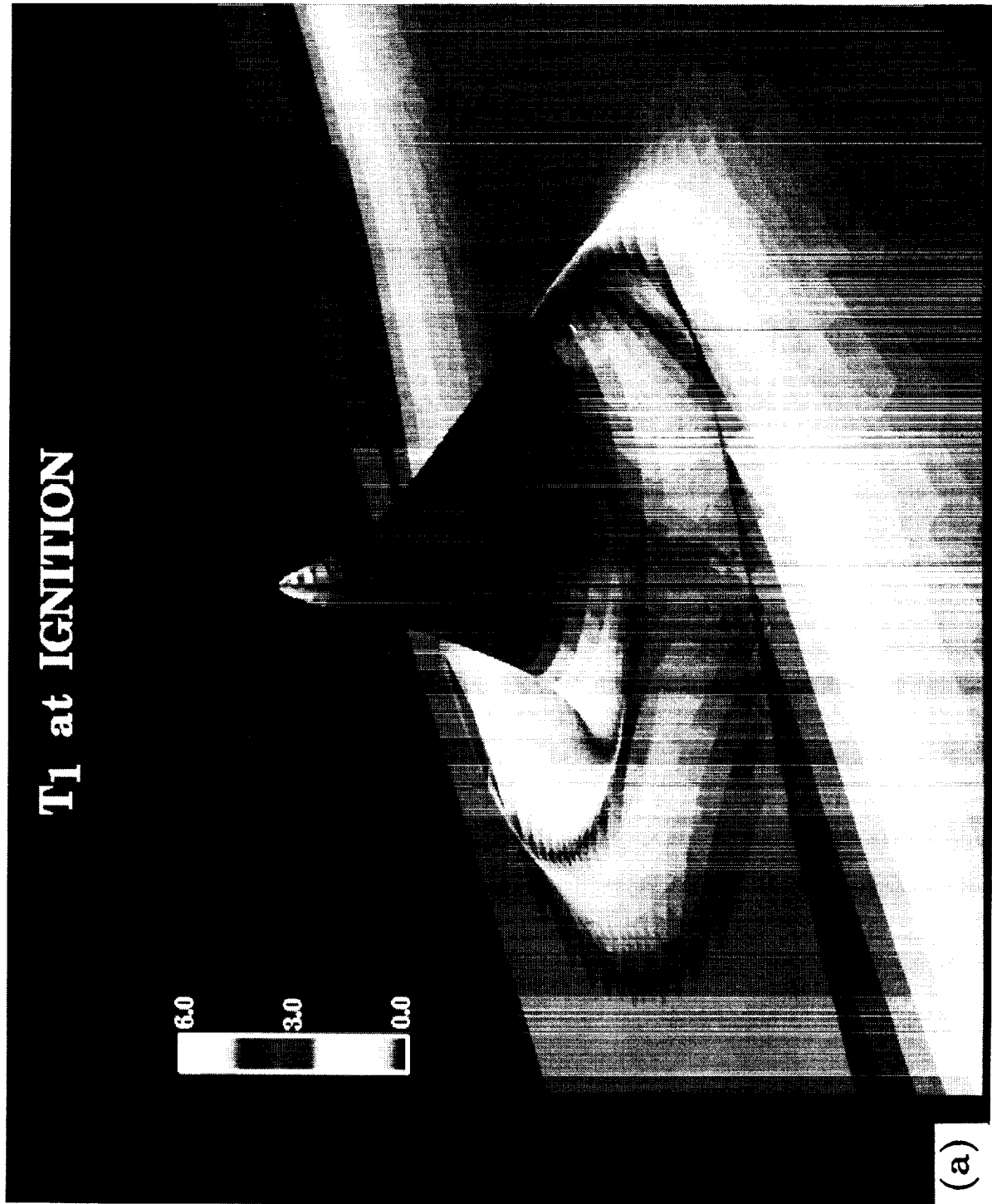
Figure 3. Surface plot of (a) T_1 and (b) $F_{1,1}$ for $R = 28.0$, $\beta_T = -2$, and $Sc = \phi = 1$.

Figure 3. Surface plot of (a) T_s and (b) $F_{1,I}$ for $R = 28.0$, $\beta_T = -2$, and $Sc = \phi = 1$.
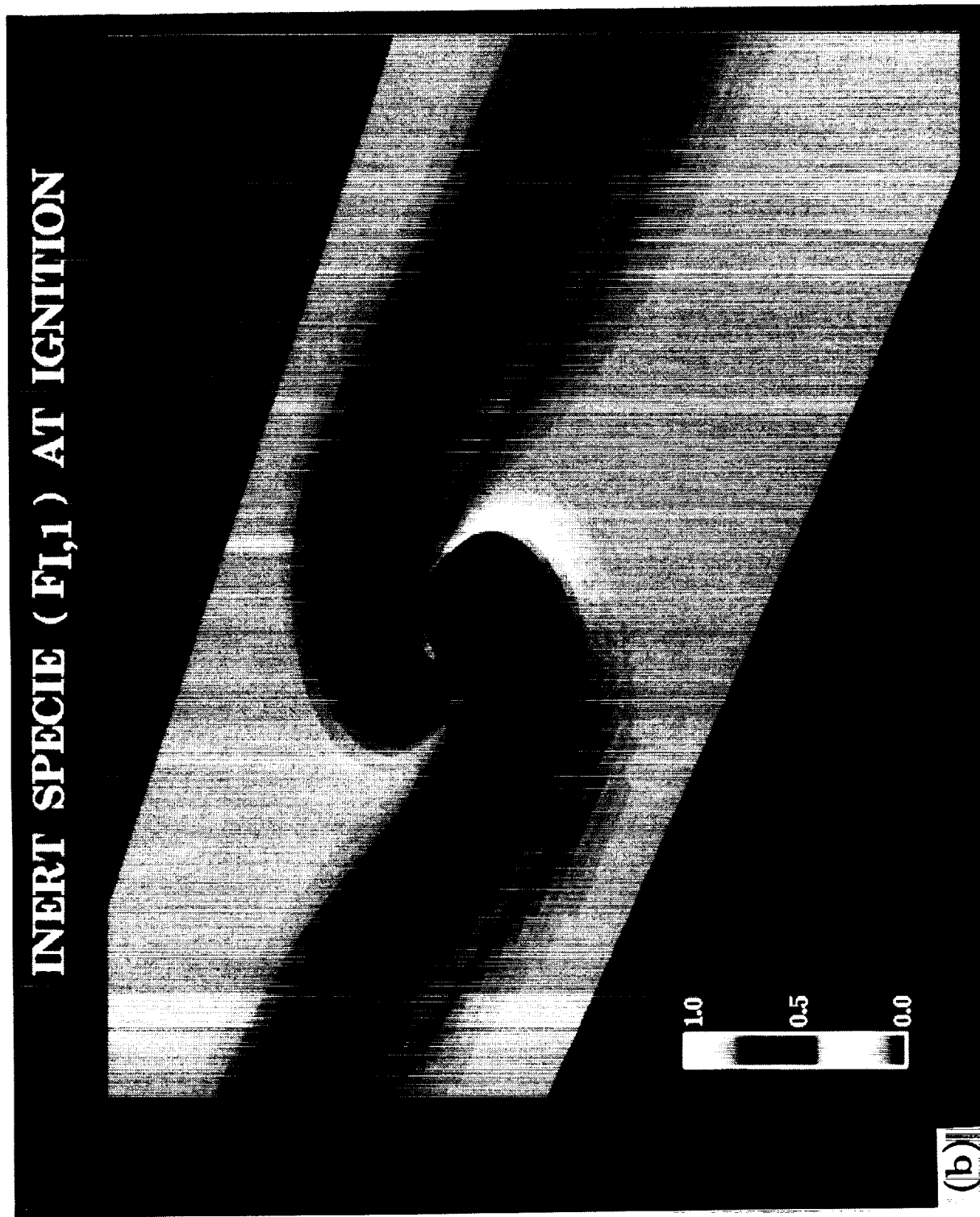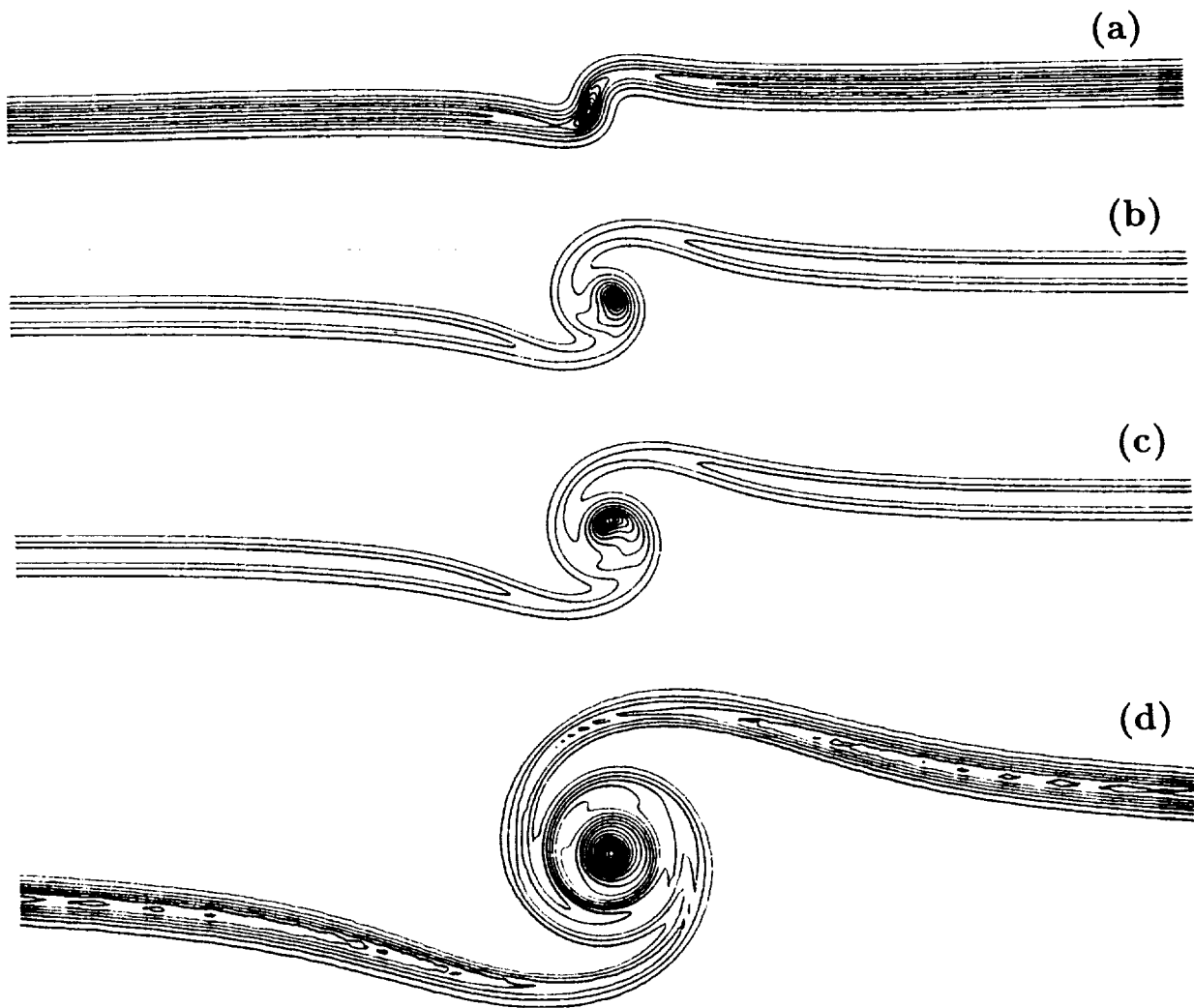
Figure 4. Contour plot of T_1 for $\bar{\beta}_\Gamma = -2$, $Sc = \phi = 1$ and (a) R = 5, (b) R = 20, (c) R = 28, and (d) R = 100.
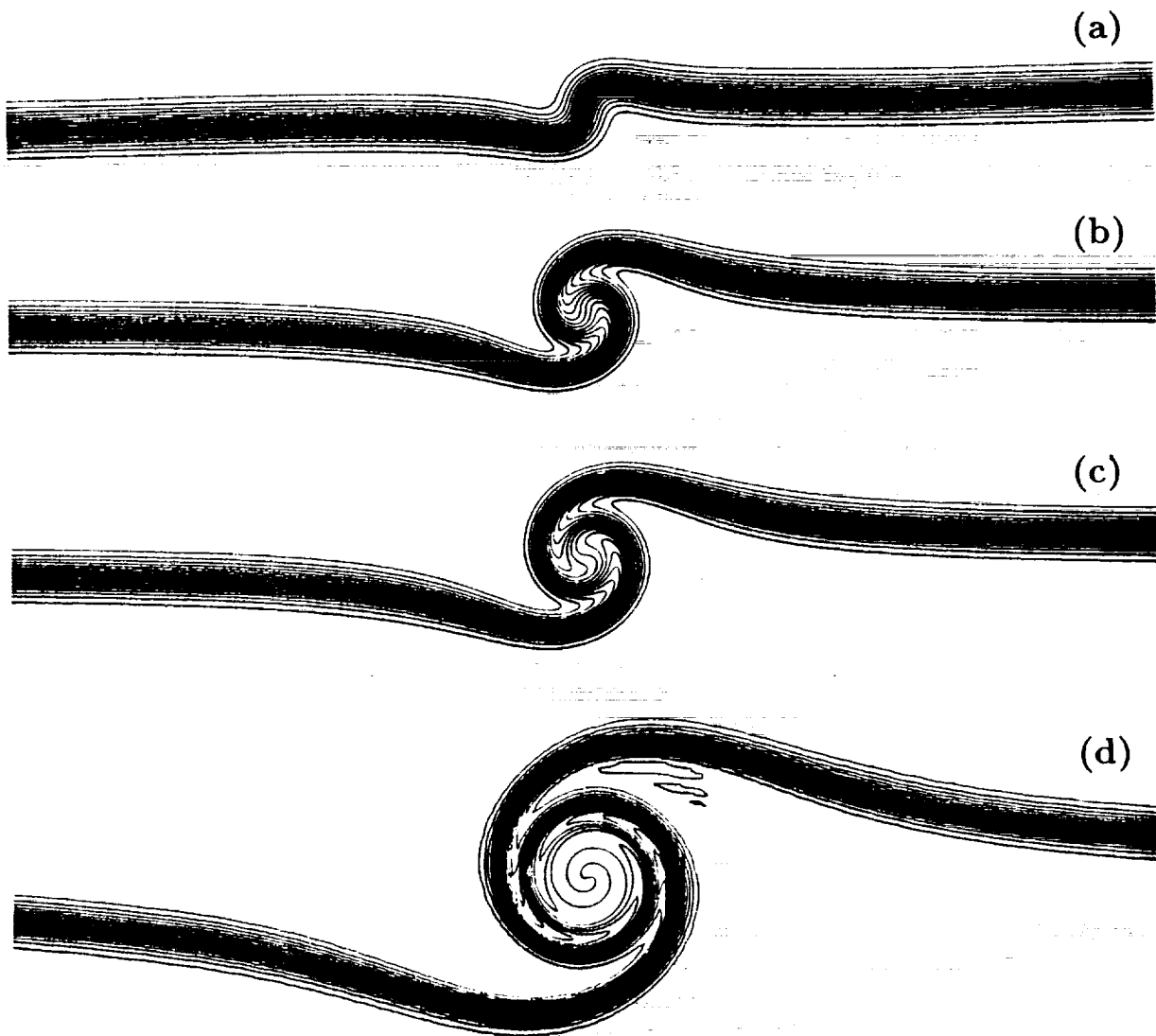
Figure 5. Contour plot of $F_{1,1}$ for $\beta_r = -2$, $Sc = \phi = 1$ and (a) $R = 5$, (b) $R = 20$, (c) $R = 28$, and (d) $R = 100$.
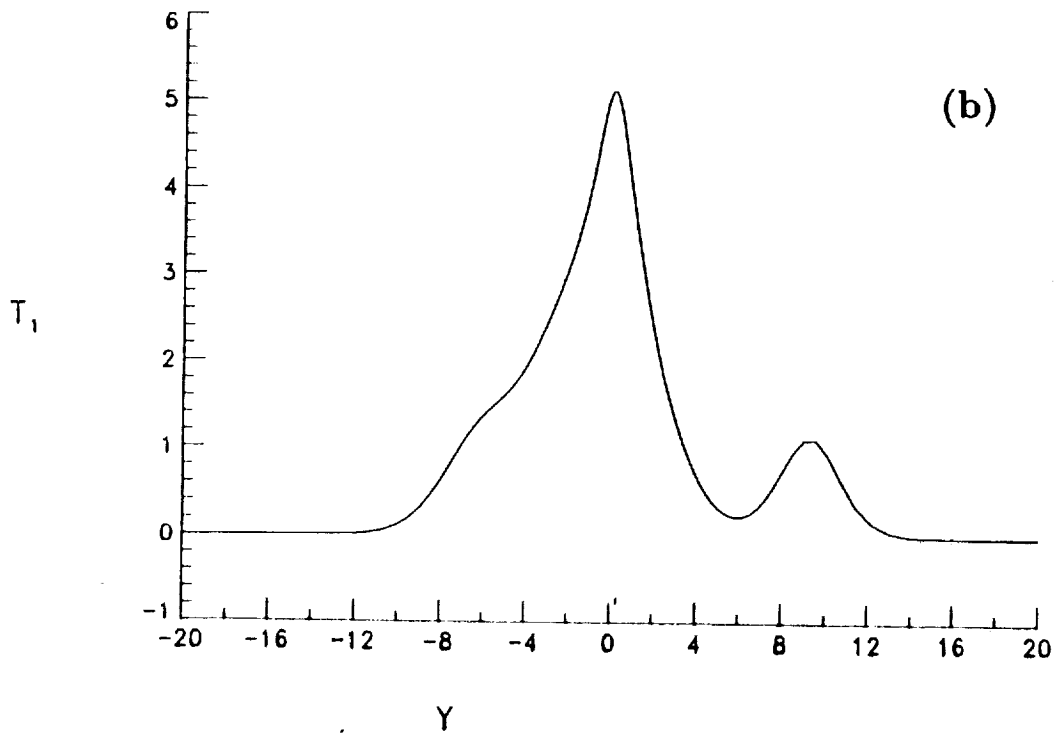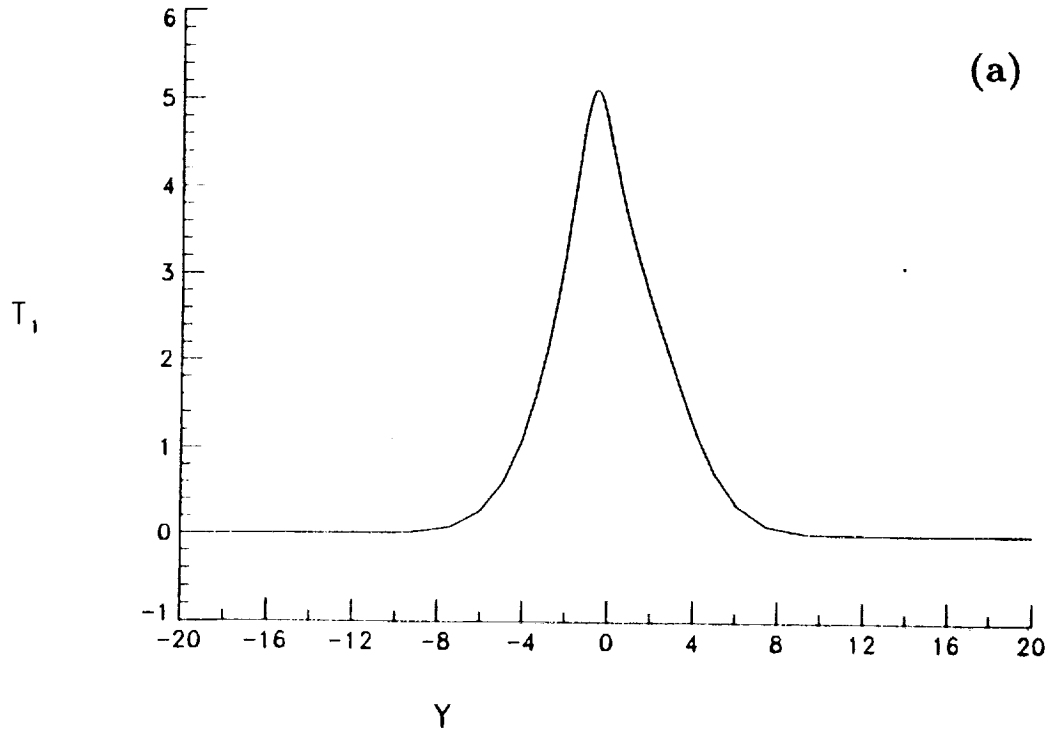
Figure 6. Plot of T_1 versus y for $\beta_T = -2$, $Sc = \phi = 1$ and (a) $R = 5$, $x_{ig} = -1.5$, $y_{ig} = -0.6886$, $t_{ig} = 12.659$; (b) $R = 20$, $x_{ig} = 2.0$, $y_{ig} = 0.0394$, $t_{ig} = 11.388$; (c) $R = 28$, $x_{ig} = 0.3466$, $y_{ig} = 1.9127$, $t_{ig} = 11.573$; and (d) $R = 100$, $x_{ig} = 0.0492$, $y_{ig} = -0.0984$, $t_{ig} = 11.466$.
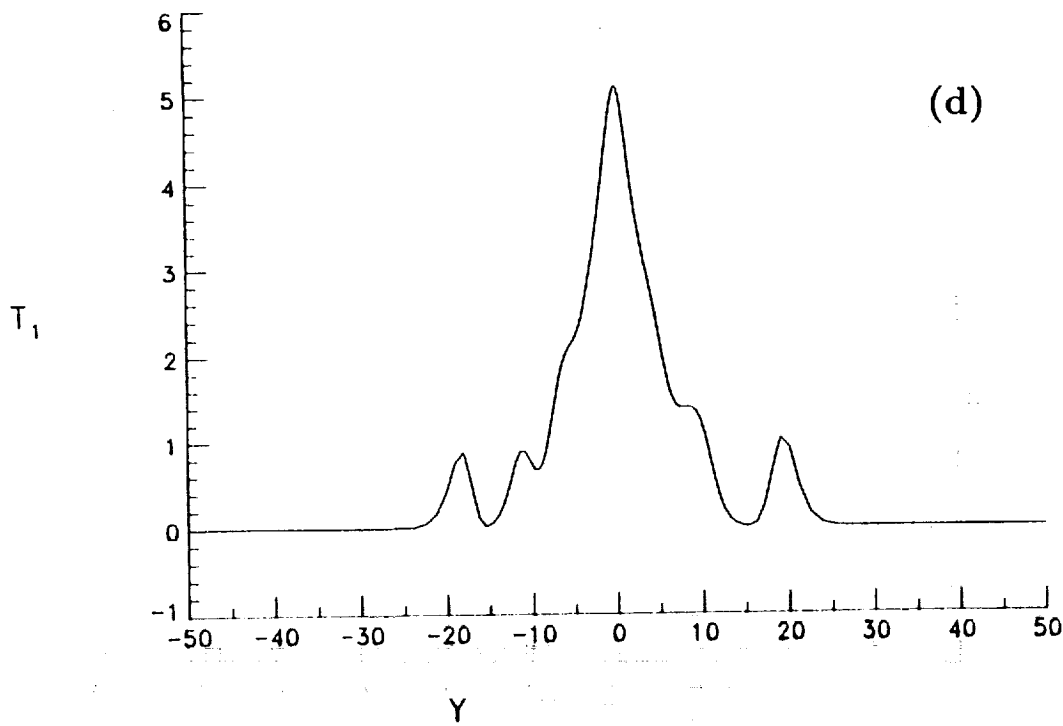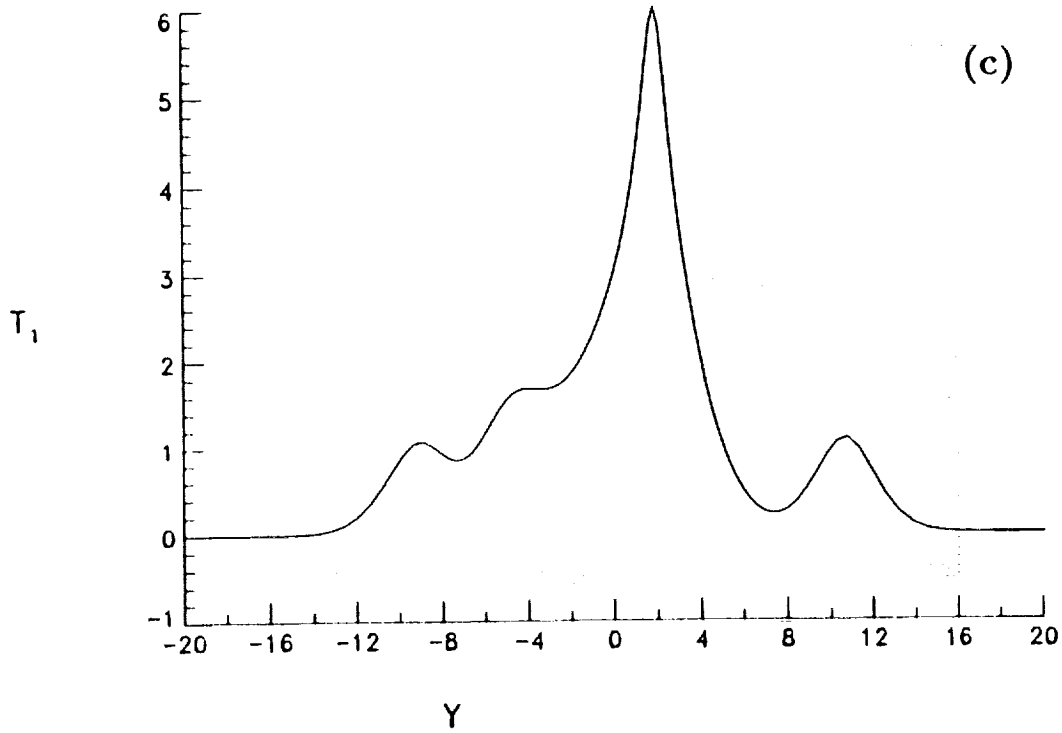
Figure 6. Plot of T_1 versus y for $\beta_T = -2$, $Sc = \phi = 1$ and (a) $R = 5$, $x_{ig} = -1.5$, $y_{ig} = -0.6886$, $t_{ig} = 12.659$; (b) $R = 20$, $x_{ig} = 2.0$, $y_{ig} = 0.0394$, $t_{ig} = 11.388$; (c) $R = 28$, $x_{ig} = 0.3466$, $y_{ig} = 1.9127$, $t_{ig} = 11.573$; and (d) $R = 100$, $x_{ig} = 0.0492$, $y_{ig} = -0.0984$, $t_{ig} = 11.466$.

Figure 7. Plot of the ignition locations y_{ig} versus x_{ig} for various values of the vortex Reynolds number with $Sc = \phi = 1$, $\tilde{\beta}_f = -2$, and using the potential vortex defined by $V = R\,Sc/r$.
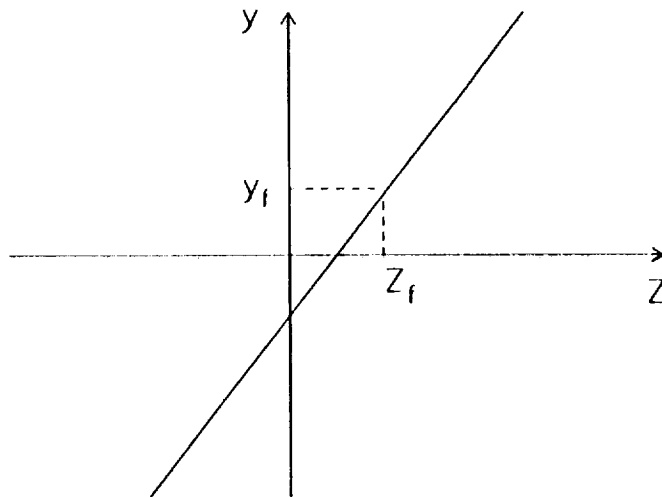
Figure 8. Schematic showing the assumed instantaneous flow field.
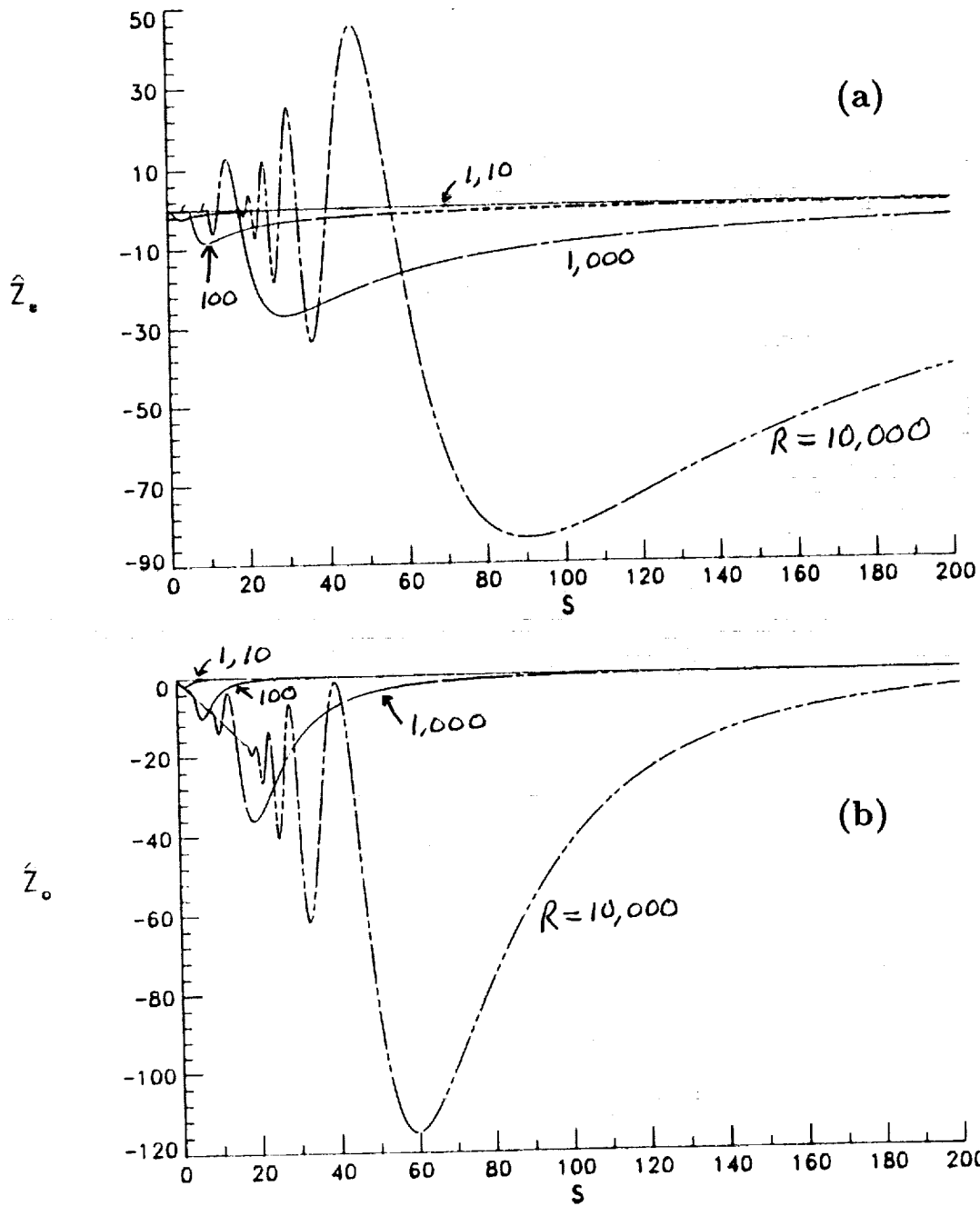
Figure 9. Plot of (a) $\hat{Z}_e$ and (b) $\hat{Z}_o$ versus s for Sc = 1 and various values of the vortex Reynolds number.
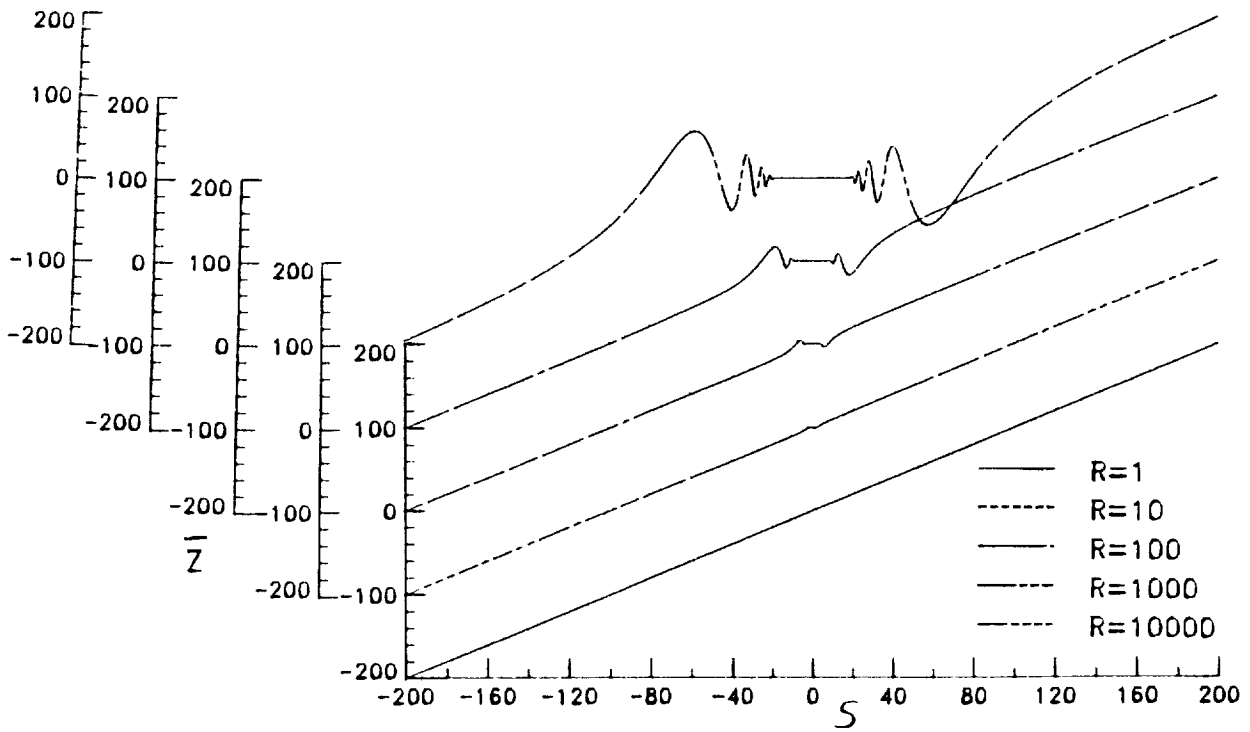
Figure 10. Plot of $\overline{Z}$ versus s for $\hat{i} = 1$, $\theta = \pm\pi/2$, $k_1 = 0$, $k_2 = 1$, $Sc = 1$ and various values of the vortex Reynolds number.
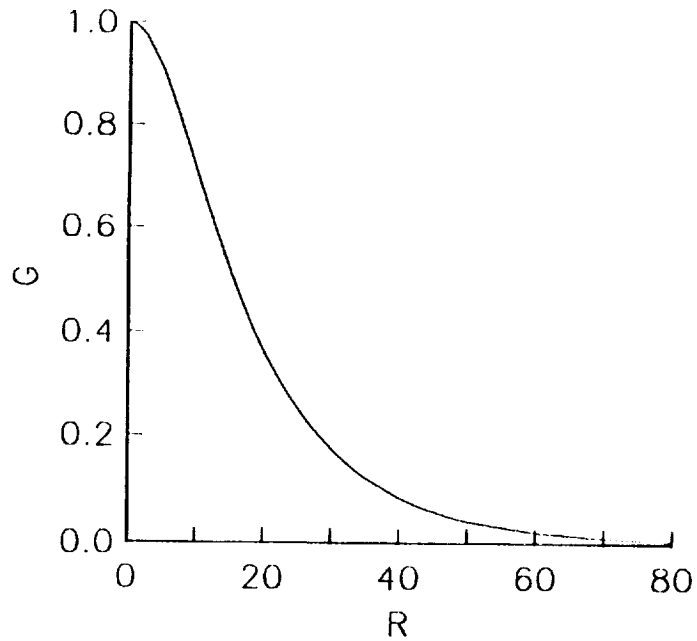

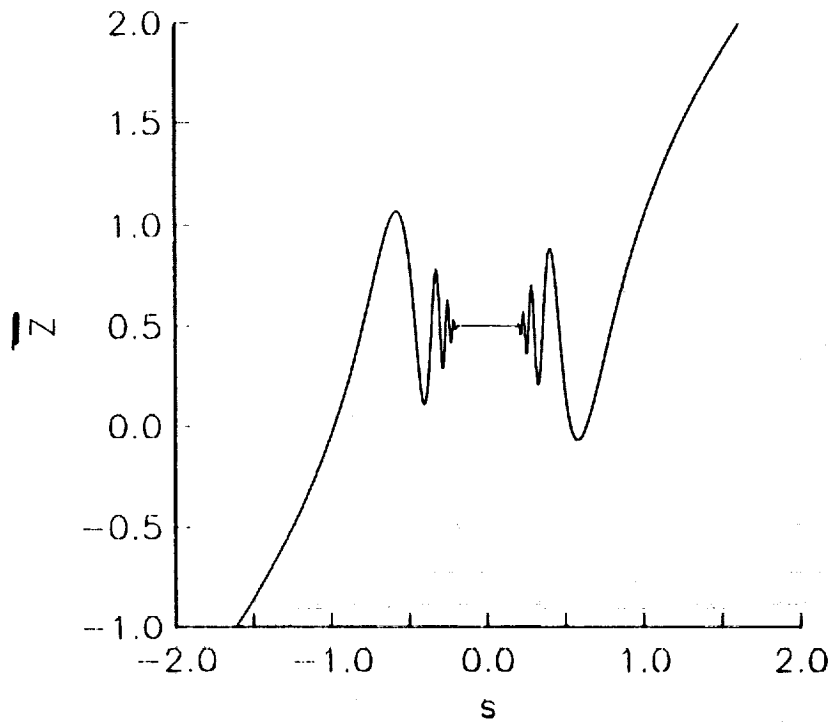Figure 11. Plot of G versus vortex Reynolds number for $Sc = \phi = k_2 = 1$.

Figure 12. Plot of the composite solution $\bar{Z}$ versus s for $\theta = \pm \pi/2$, with $k_1 = 0.5$, $k_2 = 1$, $\delta = 0.05$, and $\hat{t} = 1$.

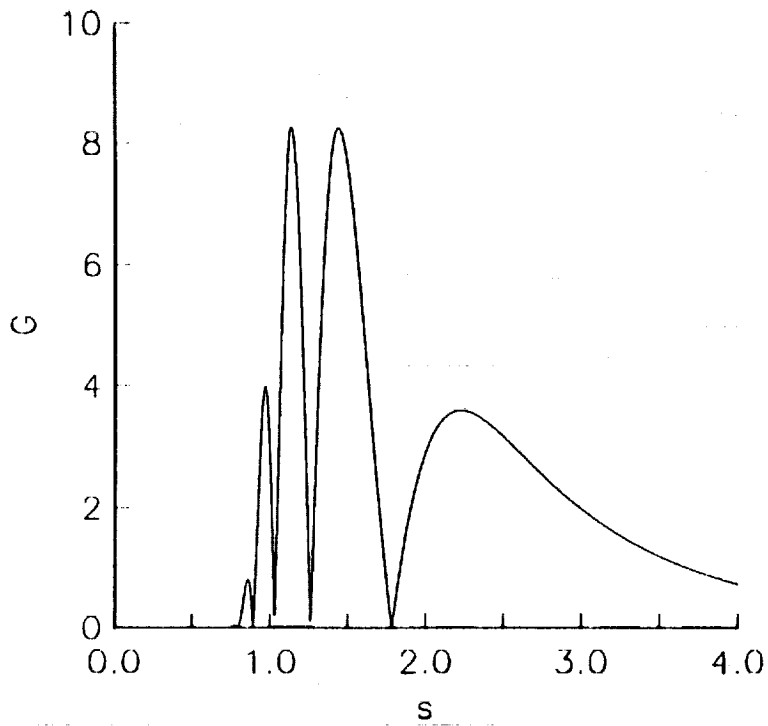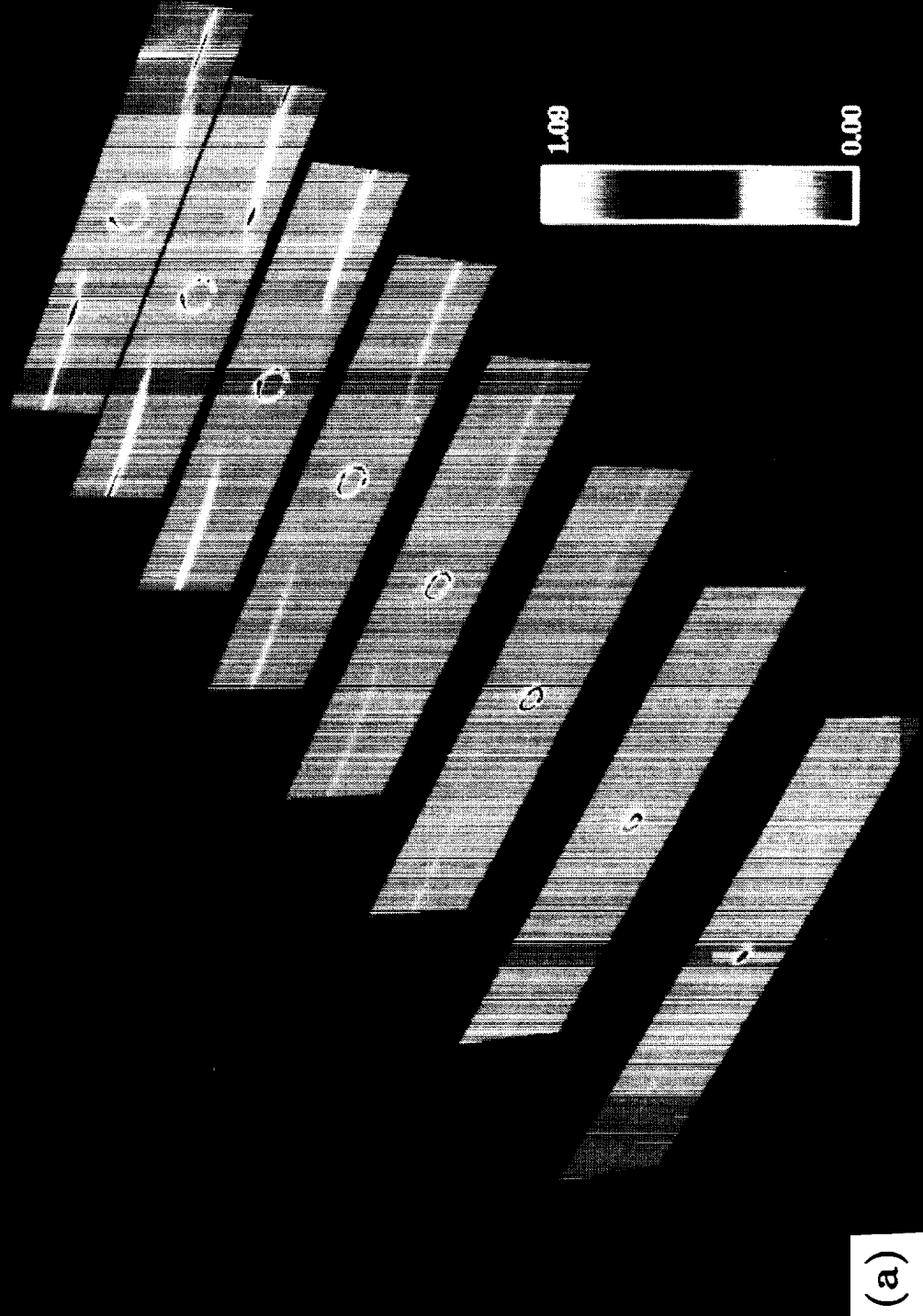Figure 13. Plot of G versus s for $\theta = \pi/2$, $k_2 = 1$, and $\delta = 1/10$.

Figure 14. Plot of the time slices of (a) the temperature profile T and (b) the reaction rate term Ω. Time increases from the bottom left corner to top right corner.
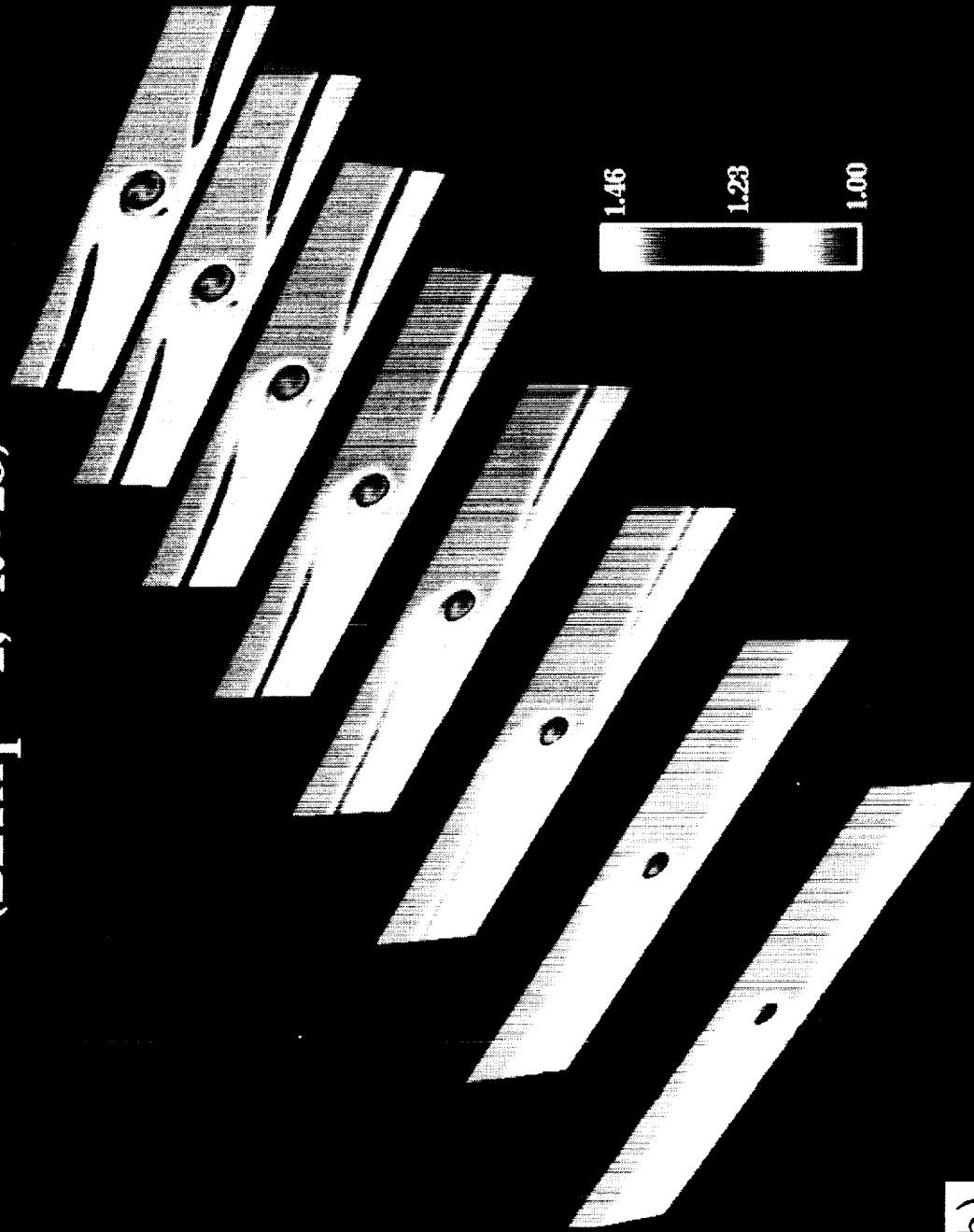
Figure 14. Plot of the time slices of (a) the temperature profile T and (b) the reaction rate term Q. Time increases from the bottom left corner to top right corner.

REPORT DOCUMENTATION PAGE

Public reporting burden for this collection of information is estimated to average 1 hour per response, including the time for reviewing instructions, searching existing data sources, gathering and maintaining the data needed, and completing and reviewing the collection of information. Send comments regarding this burden estimate or any other aspect of this collection of information, including suggestions for reducing this burden, to Washington Headquarters Services, Directorate for Information Operations and Reports, 1215 Jefferson Davis Highway, Suite 1204, Arlington, VA 22202-4302, and to the Office of Management and Budget. Paperwork Reduction Project (0704-0188), Washington, DC 20503.

1. AGENCY USE ONLY (Leave blank)	2. REPORT DATE September 1991	3. REPORT TYPE AND DATES COVERED Contractor Report

4. TITLE AND SUBTITLE	5. FUNDING NUMBERS
Ignition and Structure of a Laminar Diffusion Flame in the Field of a Vortex	C NAS1-18605 WU 505-90-52-01
6. AUTHOR(S) Michéle G. Macaraeg, T.L. Jackson, and M.Y. Hussaini	

7. PERFORMING ORGANIZATION NAME(S) AND ADDRESS(ES)	8. PERFORMING ORGANIZATION REPORT NUMBER
Institute for Computer Applications in Science and Engineering Mail Stop 132C, NASA Langley Research Center Hampton, VA 23665-5225	ICASE Report No. 91-69

9. SPONSORING/MONITORING AGENCY NAME(S) AND ADDRESS(ES)	10. SPONSORING/MONITORING AGENCY REPORT NUMBER
National Aeronautics and Space Administration Langley Research Center Hampton, VA 23665-5225	NASA CR-189545 ICASE Report No. 91-69

11. SUPPLEMENTARY NOTES
Langley Technical Monitor: Michael F. Card Final Report Submitted to Combustion Science & Technology

12a. DISTRIBUTION/AVAILABILITY STATEMENT	12b. DISTRIBUTION CODE
Unclassified – Unlimited Subject Category 25	

13. ABSTRACT (Maximum 200 words)

The distortion of flames in flows with vortical motion is examined via asymptotic analysis and numerical simulation. The model consists of a constant-density, one-step, irreversible Arrhenius reaction between initially unmixed species occupying adjacent half-planes which are then allowed to mix and react in the presence of a vortex. The evolution in time of the temperature and mass-fraction fields is followed. Emphasis is placed on the ignition time and location as a function of vortex Reynolds number and initial temperature differences of the reacting species. The study brings out the influence of the vortex on the chemical reaction. In all phases, good agreement is observed between asymptotic analysis and the full numerical solution of the model equations.

14. SUBJECT TERMS			15. NUMBER OF PAGES 34
ignition; vortex; laminar diffusion flame			16. PRICE CODE A03

17. SECURITY CLASSIFICATION OF REPORT Unclassified	18. SECURITY CLASSIFICATION OF THIS PAGE Unclassified	19. SECURITY CLASSIFICATION OF ABSTRACT	20. LIMITATION OF ABSTRACT

NSN 7540-01-280-5500